Axial Structure of Fast Spreading Mid-Ocean Ridges:

Implications for Overlapping Spreading Centers

by

Donna Kay Blackman
B.S. University of California, 1982

SUBMITTED TO THE DEPARTMENT OF EARTH,
ATMOSPHERIC AND PLANETARY SCIENCES
IN PARTIAL FULFILLMENT OF THE
REQUIREMENT FOR THE DEGREE
OF

MASTER OF SCIENCE in MARINE GEOPHYSICS
at
MASSACHUSETTS INSTITUTE OF TECHNOLOGY
September 1986

Signature of Author _____
Joint Program in Oceanography, Woods Hole
Oceanographic Institution/Massachusetts
Institute of Technology

Certified by _____
Hans Schouten — Co-Thesis Advisors at W.H.O.I. — Peter Meyer

Certified by _____
Thesis Supervisor at M.I.T. Marcia McNutt

Accepted by _____
Chairman, William Brace
Departmental Graduate Committee

Axial Structure of Fast Spreading Mid-Ocean Ridges: Implications for Overlapping Spreading Centers

by
Donna Blackman

Abstract

Studies of the structure of mid-ocean ridges and the processes involved at these accreting plate boundaries have played an important role in the development of plate tectonics models over the last two decades. During this time our concept of the accretion/spreading process has evolved from a two-dimensional, steady-state picture to a three dimensional, time-dependent view of the volcanism and rifting. Using the axial morphology of a fast spreading mid-ocean ridge as a constraint, isostatically balanced density structures, representing the central portion of a ridge segment, the off-axis region and the ridge tip at an overlapping spreading center, are determined for two end member models. One emphasizes the role of the subaxial asthenosphere in maintaining axial ridge topography. The other emphasizes the role of a crustal magma chamber.

The results of mass balance calculations that are consistent with gravity data indicate that both models are viable in terms of their ability to support an axial ridge of the size observed along the East Pacific Rise (EPR). Isostatic support of a 300-400 m high axial ridge requires either subaxial asthenospheric melt contents of 10-25% or a 2.5-4.0 km thick magma chamber.

Axial ridge volumes are shown to range from 1×10^6 to 5×10^6 m^3/m along the EPR, with significant decreases at overlapping spreading centers. The volume of subaxial asthenospheric melt required to balance a ridge of a given volume is less than half that required in a crustal magma chamber where the density contrast between the melt and its surroundings is considerably less. Gravity and petrologic data suggest that a large magma chamber is unlikely to be maintained along the EPR. Although it is not presently possible to put strict limits on the maximum size of the axial magma chamber, there is some evidence that the shallower sections of the EPR axial ridge may not be supported solely by low density material in the crust.

Thesis Supervisors: Hans Schouten, Associate Scientist
Peter Meyer, Assistant Scientist

Acknowledgements

A number of factors, both scientific and otherwise, have contributed to the making of this thesis. Credit for the initial scientific inspiration goes to Jeff Karson during whose three hour long descriptive lectures on ophiolites and oceanic lithosphere I had to find something to think about just to stay awake. Trying to understand the depth variation of mid-ocean ridge crests that Jeff described kept me awake during the course and has kept me occupied for much of the past 20 months. Discussions with both Hans Schouten and Peter Meyer have helped me expand and better organize the ideas I started with. The combination of geophysical and petrological expertise in these advisors served to bring together arguments from both 'camps' and has provided an interesting environment for this work. Thanks go to Jeff Fox, Bob Ballard and Peter Lonsdale for providing preprints of manuscripts and copies of SEABEAM data and axial depth profiles along the East Pacific Rise.

Of the nonscientific contributors to this thesis, the greatest acknowledgement goes to Richard, interactions with whom I've allowed to significantly influence my past two years. If our paths had crossed at a different time or place, this project might not have evolved as a masters thesis. Yet, I've learned a lot in pulling this work together here and for that, as well as other things less tangible, I am grateful.

During my enrollment as a Joint Program student I have been financially supported by Educational Fellowships from Woods Hole Oceanographic Institution and, for one term, by an ONR grant under Hans Schouten.

Table of Contents

List of Figures

List of Figures (cont.)

List of Figures (cont.)

List of Figures (cont.)

1. Introduction

The purpose of this study is to examine the structure of fast spreading mid-ocean ridges (MORs) and to assess the possible roles of the subaxial asthenosphere compared with that of a crustal magma chamber in maintaining the ridge structure. The route by which a basaltic melt, generated at depth, buoyantly rises and eventually becomes part of the oceanic crust is not presently understood. A first step in unraveling the processes controlling this sequence is to determine models for the melt distribution within the mid-ocean ridge system. When lower density melt is present in significant amounts it will affect the surface morphology which must adjust to the underlying density structure. Given some constraints on the distribution of melt within the system, it should be possible to make some inferences as to the physical processes that control the axial morphology. The approach taken here is to quantify the variations in axial bathymetry both along and across-strike and, assuming isostatic compensation, to find the range of reasonable density structures that might result from variations in asthenospheric melt content, size of a crustal magma chamber, or changes in the thickness of the axial crust.

Previous models of MOR structure tend to focus on either the deeper region, with the form of mantle upwelling being investigated, or the shallow region, where crustal strength or magma chambers are shown to be important factors. Although this separation in emphasis of earlier models mainly reflects the approach of a given study (analytic vs observational, for example) and is, therefore, an artificial division of the system, it is useful to approach the study of MOR by breaking the

system into two 'components': 1) subaxial asthenosphere, through which melt formed at depth must transit; 2) lithosphere (consisting mainly of crust at the ridge axis), which may store large amounts of melt in axial magma chambers. The range of topography for which one of these 'components' is the dominant influence on ridge structure vs the other can be determined by separately investigating the possible contribution of each. Two simple models are chosen to represent this. Model 'A' comprises concepts from earlier models of subaxial mantle upwelling in an attempt to focus on the subcrustal region of MORs. Crustal structure as a function of the size or presence of a magma chamber is represented in model 'B'. These models form the basis for the isostatic calculations in section 4. In addition to general fast spreading ridge morphology, the characteristic morphology of at Overlapping Spreading Centers (OSCs) is used as a constraint in exploring the possible contribution of each end member model.

General Morphology of fast spreading MORs. The general morphology of fast spreading mid-ocean ridges (the EPR is the prime example) consists of a broad high that deepens away from the axis according to the $\sqrt{t}$ cooling curve. Superimposed on the broad swell is a narrow axial ridge that typically stands 200-400 m higher (Figure 1.1; Lonsdale, 1977a; Klitgord and Mammerickx, 1982). The width of the axial ridge varies from 2 to 15 km. Along-strike, the EPR is composed of several ridge segments that are offset at either transform zones or OSCs. Axial depths are generally least near the center of segments (mid-segment highs) and increase 200-400 m towards the offsets (Figure 1.2). In this study, possible structural changes from the mid-segment high to the

ridge 'tip' are considered.

Any model of mid-ocean ridges must incorporate or assume some form of basaltic melt generation, crustal extension, extrusion of material at the seafloor and accretion of lithospheric plates. Previous models of MOR structures and dynamics can be divided into two classes: those that focus on the subcrustal region of MOR and those that focus on the crustal region.

Subaxial Asthenosphere models. Early models (eg. Sleep, 1969) attempted to explain the morphologic differences between fast and slow spreading centers by the existence of a broad vs narrow zone of asthenospheric upwelling (assuming a negligible crustal constribution and without specifying the form of asthenospheric motion). Sleep (1969) could not distinguish between the two models (narrow vs broad upwelling) on the basis of heat flow or gravity but was able to use the difference in morphology at fast vs slow spreading centers to introduce a model that showed the potential importance of the viscosity of upwelling asthenosphere as an influence on the morphology of the ridge axis. He suggested that significant viscous head loss could result if the width of the upwelling region was narrow as was expected for slower spreading rates. The model was further developed to explain the increased axial depths at ridge-transform intersections (Sleep and Biehler, 1970). Lachenbruch (1973) also considered the effect of asthenospheric upwelling on topography in a model of passive spreading. The buoyant rise of material through an axial conduit in rigid lithosphere was shown (Lachenbruch, 1973; 1976) to be balanced by a combination of the pressure of water above the conduit and shear stresses generated at the

conduit walls (the plate edge). He suggested that upwelling occurs across a width of the order of 15 to 20 km at fast spreading centers. This width is not consistent with the narrowness of the axial ridge (that not explained by the $\sqrt{t}$ cooling curve). This discrepancy suggests that although the concepts developed by Sleep and Lachenbruch are quite useful, further study is required in order to address the narrow region at the ridge axis. (Although the main focus of his discussion was the large scale ridge morphology, Lachenbruch (1973) did suggest that a similar mechanism of confined viscous flow could explain smaller scale horsts and grabens as well.) Rea (1975) used the conduit model of Lachenbruch (1973) to explain the height of the narrow axial 'block' of the EPR near 10°S. He noted the problem of the excessive width predicted by Lachenbruch's model for the axial conduit but proceeded to apply it in concept to explain the morphology of the ridge axis and the development of off-axis rotational faults to create the abyssal hills.

The above models address cross-strike ridge structure. Variability in subaxial asthenosphere properties will also affect along-strike ridge morphology. In the last few years high-resolution data has revealed the three-dimensional nature of ridge structure and studies have been devoted to explaining along-strike variability. Generally these models can be thought of in superposition with across-strike models, the processes at a given point along a ridge segment appearing time-dependent, reflecting 'cycles' of magmatic activity.

The observed segmentation of mid-ocean ridges, and its apparent consistency through time, has inspired recent studies that suggest that

subaxial mantle upwelling may be localised by a mechanism similiar to a Rayleigh-Taylor gravitational instability. Whitehead et al. (1984) used a simple laboratory experiment to show that a thin zone of buoyant material will develop regularly spaced instabilities into which melt will be channelled to form blobs that rise through a more viscous surrounding material. Crane (1985) independently arrived at a similiar conclusion based on the rather regular spacing of transform faults along a given ridge. She inferred that the cooler regime associated with a ridge-transform intersection would influence the thermal properties of the deeper mantle and give rise to Rayleigh-Taylor instabilities in a melt zone at depth. She qualitatively showed the dependence of ridge segment length on spreading rate noting that transform spacing, and therefore the spacing of upwelling regions, is greater at fast spreading ridges. Schouten et al. (1985) further developed an instability model to incorporate estimates of upper mantle viscosity, melt content of the asthenosphere below the ridge and a time constant for magmatic activity. They showed that on average the distance between mid-points of spreading segments could be a function of spreading rate to the 1/3 power.

Before concluding this section on subcrustal structure, along-strike migration of magmatic activity needs to be addressed. Again, the variation of processes along the axis of a ridge segment may determine the cross-strike structure at a given location through time. And, the notion of longitudinal variation in ridge structure may strongly depend on some sort of propagation of the system as whole. Parmentier and Forsyth (1985) present a model of horizontal

asthenospheric flow in an axial conduit terminating against the cold plate edge at a transform fault. Their model was developed to explain the morphology observed at the Mid-Atlantic Ridge (MAR) but the concept is useful at any mid-ocean ridge. The along-strike flow of asthenosphere is predicted to cause the deepening of the rift valley over several tens of kilometers, a result that is not achieved by thermal conduction models at ridge-transform intersections (Forsyth and Wilson, 1984).

Phipps-Morgan and Parmentier (1985) attempt to explain the axial bathymetry of Propagating Rifts (PR) associated with hot spots. They suggest that rift propagation is driven by the excess topography of the ridge axis and that the driving force is approximately counterbalanced by subaxial asthenospheric flow. The steepness of the ridge tip can be explained if it is supported dynamically by viscous flow in a subaxial conduit that terminates at the propagating tip. The model itself is limited to simple geometries (symmetric off-axis topography) and the reference depth used to calculate the driving and resisting forces is not well defined but, again, the concept is valid and may be applied at the ridge segments of the EPR which, in a self-similar sense, show the same dropoff of axial bathymetry towards their tips.

Schouten et al. (submitted) base a model of along-axis migration of mid-ocean ridge magmatism on the V-shaped non-transform trends of off-axis bathymetric features. The off-axis coverage tends to be limited but linear trends of seamounts and/or regions of anomalously rough topography can be traced back to the present location of axial highs and/or segment terminations. The interpretation is that narrow

regions of mantle upwelling are overridden by the spreading centers giving both an across and an along-axis component of motion relative to the ridge axis.

In summary, previous models of MOR structure that focus on the subaxial asthenosphere predict a rather narrow zone of upwelling in which melt generated at depth rises to become axial crust. Different authors propose different modes or geometries of upwelling and most explain the general features of MORs well but lack detail or accuracy near the axis. Variation in the supply of melt from depth has been hypothesized to explain along-strike undulations of ridge topography.

Crustal Magma Chamber models. The models reviewed below examine the structure of the upper 5-7 km of the MOR system. Although generally not explicitly mentioned, previous crustal models implicitly assume that subcrustal properties have a negligible effect on the surface expression of a MOR. What this amounts to is an assumption that the passage of melt through the asthenosphere occurs rapidly (on the scale of the response time of the ridge to changes in underlying density structure) and that no large accumulations of melt exist below the crust.

Crustal models most often pursue the problem of an axial magma chamber and its petrologic, gravity and/or topographic effects. One class of crustal models, though, focuses on the strength of the axial lithosphere and its behavior under extension as evidenced by the ridge axis morphology. These models (eg. Tapponier and Francheteau, 1978; Emerman and Turcotte, 1984), considered in conjunction with the Sleep (1969) or Lachenbruch (1973) models, could alleviate the requirement of excessively wide conduits (see previous subsection). Steady-state

necking models describe a lithosphere that thins to 4 or 5 km thickness at the MOR axis due to extension. Tapponier and Francheteau (1978) show that, for reasonable assumptions of the material properties of this necking lithosphere, the axial valley at slow spreading MORs can be explained without resorting to arguments of viscous resistance in a narrow region of upwelling. By neglecting the possible contribution of the crustal component of the ridge, the subcrustal conduit models were forced to account for both the deep axial valley at slow spreading centers and the axial ridge at fast spreading centers with the same criteria. If the thickness or properties of the axial lithosphere are a function of spreading rate as proposed by Tapponier and Francheteau (they indicate that the asthenosphere should play the dominant role at faster spreading ridges where they believe lithosphere to be thinner and weaker) then the application of the same criteria to fast spreading ridges as to slow is not appropriate. Emerman and Turcotte (1984) also investigate a steady-state necking model. They assume that the lithosphere is about 5 km thick at all spreading ridges but that the morphology depends on the differing rates at which lithospheric viscosity increases away from the axis with respect to the corresponding decrease in rate of accretion. They show that the broad swell at the EPR can be explained this way, yet they do not attempt to explain the details of the axial region.

In contrast to the above models involving asthenospheric conduits and lithospheric rigidity, the EPR Study Group (1981) prefers to explain the morphology of the ridge as an expression of a 20 to 30 km wide crustal magma chamber which is isostatically compensated. In a review

of several types of data they attempt to show that the observations cannot be explained without the existence of an axial magma chamber along the EPR. These data include: the small positive gravity anomaly over MORs that can be modeled by a thin plate buoyed by underlying low density material; the existence of axial low velocity regions determined by synthetic seismograms which fit seismic refraction and reflection data; compostional variation of mid-ocean ridge basalts (MORB) and the subaxial existence of plutonic rocks. They present convincing geochemical evidence for magma mixing, assumed to occur in a crustal magma chamber. They also show that the zone of active intrusion is quite narrow, based on magnetics studies. Finally, the EPR Study Group (1981) show the ubiquity of hydrothermal circulation along the ridge axis which strongly influences the thermal regime of the upper few kilometers.

Seismic reflection data from just north of the 9°03'N OSC show a reflector that has a phase reversal indicative of the presence of melt below the interface. Hale et al. (1982) show that low velocity material underlies the upper axial crust (about 1 sec below the seafloor) on the western flank of the ridge north of the OSC. They suggest that this marks the top of a crustal magma chamber.

More recently collected multichannel seismic reflection data from the EPR, 9°-13° N, show continuous, strong reflectors at depths of 1-2 km. Detrick et al. (1986) interpret the reflector, which shows a phase reversal in some places, as the top of an axial magma chamber. Cross-axis profiles in their data constrain the width of the low velocity region to 4-5 km.

Thermal models and ophiolite-based models suggest that a much broader axial magma chamber is present at mid-ocean ridges. For fast spreading rates, thermal models predict that the chamber should be about 20 to 30 km wide (Sleep, 1975; Sleep and Rosendahl, 1979) in agreement with the sizes determined from ophiolite sequences (eg. Pallister and Hopson, 1981). Although the former models are able to fit the topography of the ridges fairly well, the width of the assumed magma chamber is inconsistent with recent multichannel seismic results that indicate a low velocity zone of only 4 km width beneath the EPR (Hale et al., 1982; Detrick et al., 1986). Gravity modeling also implies that low density material is 'concentrated' within 5 km of the ridge axis (Madsen et al., 1984). It is possible, though, that the apparent inconsistency between the seismic data and thermal or ophiolite models can be resolved if crystallization within the magma chamber results in only a small region of very high melt content. If the density contrast between this and surrounding parts of the chamber is greater than that between the cumulate mush layers and the adjacent lithosphere, there would be no reason to expect a strong reflector at the chamber edge

Along-strike variation of magmatic processes and ridge topography have been attributed to differences in the size or stage of evolution of an axial magma chamber. Francheteau and Ballard (1983) proposed a model in which a central magma chamber is cooled at its edges by abutting cold lithosphere across a tranform fault. They suggested that the axial high of a ridge segment corresponds to greater volume of low density magma. The simplest interpretation of their model would predict a symmetric axial depth profile about the center of a segment with the shallowest

point approximately mid-way between transform faults of equal offset, but this is not what is observed (see Figure 1.2 and Macdonald et al., 1984).

Continuous SEABEAM coverage of the EPR axis from 8°-14° N clearly shows along-strike changes in ridge morphology. Macdonald et al. (1984) interpret these data as evidence of the waxing and waning of the magmatic budget along the ridge. They suggest that shallow ridge sections reflect an inflated magma chamber and should be associated with very active volcanism. Conversely, the deeper sections should be less active volcanically and more tectonized as Macdonald et al. (1984) claim to be the case at many ridge segment terminations.

Two end-member models of subaxial ridge structure. Cartoons of the two models considered are shown in Figure 1.3. Model 'A' assumes pressure release melting at depth. Less dense asthenosphere, resulting from the melt within its matrix, rises buoyantly in a narrow zone below the ridge axis. The cartoon is intended to show a time averaged picture of the velocity in the upwelling region. The velocity dropoff is rather sharp at the edges of the upwelling zone and therefore effectively produces a vertical walled conduit. Thin crust overlies the asthenosphere in the conduit but it is assumed to be of low strength and to adjust relatively freely to the underlying density structure. Lithospheric accretion, other than that due to extrusion at the ridge axis, occurs along the sides of the conduit. In the cartoon, the axial crust is depicted as being approximately the same thickness on and off-axis. The effect of the assumed thickness on the ridge structure is discussed in section 4. Along-axis variations in the asthenospheric melt content, and therefore

viscosity, are assumed to result from Rayleigh-Taylor type gravitational instabilities that impinge on the crust beneath the axial high of a ridge segment.

Model 'B' depicts a crust approximately constant in thickness across the axial region. A magma chamber is present and assumed to be of a width on the order of the axial ridge width and to reach to within 1 to 2 km of the surface. In this case it is assumed that the properties of the underlying asthenosphere do not significantly influence the surface morphology (see discussion in subsection on crustal magma chamber models) and, therefore, they remain unspecified. Crustal accretion takes place along the walls, floor and ceiling of the magma chamber. Near the terminations of a ridge segment the chamber is assumed to pinch out as a result of lower temperatures there.

Constraints on the possible range of density structures corresponding to each of the two models are developed in section 4. These will incorporate both along-strike and across-strike scenarios. In order to avoid the certain complications at ridge-transform intersections (distinct differences in the thermal structure across the transform) only morphologies that relate to segments that terminate at OSCs are considered. It is not yet clear from previous studies of OSCs (Macdonald and Fox, 1983; Lonsdale, 1983, 1985; Macdonald et al., 1984) whether or not the axial thermal structure near OSCs is as distinct as that near fracture zones. This question is implicitly addressed by the various assumed density structures (Section 4) which will certainly be a function of the local thermal regime.

In order to establish the scale of the bathymetric variations along ridge segments bounded by OSCs, the following section is devoted to a brief review of previously published data and more detailed analyses of the SEABEAM data.

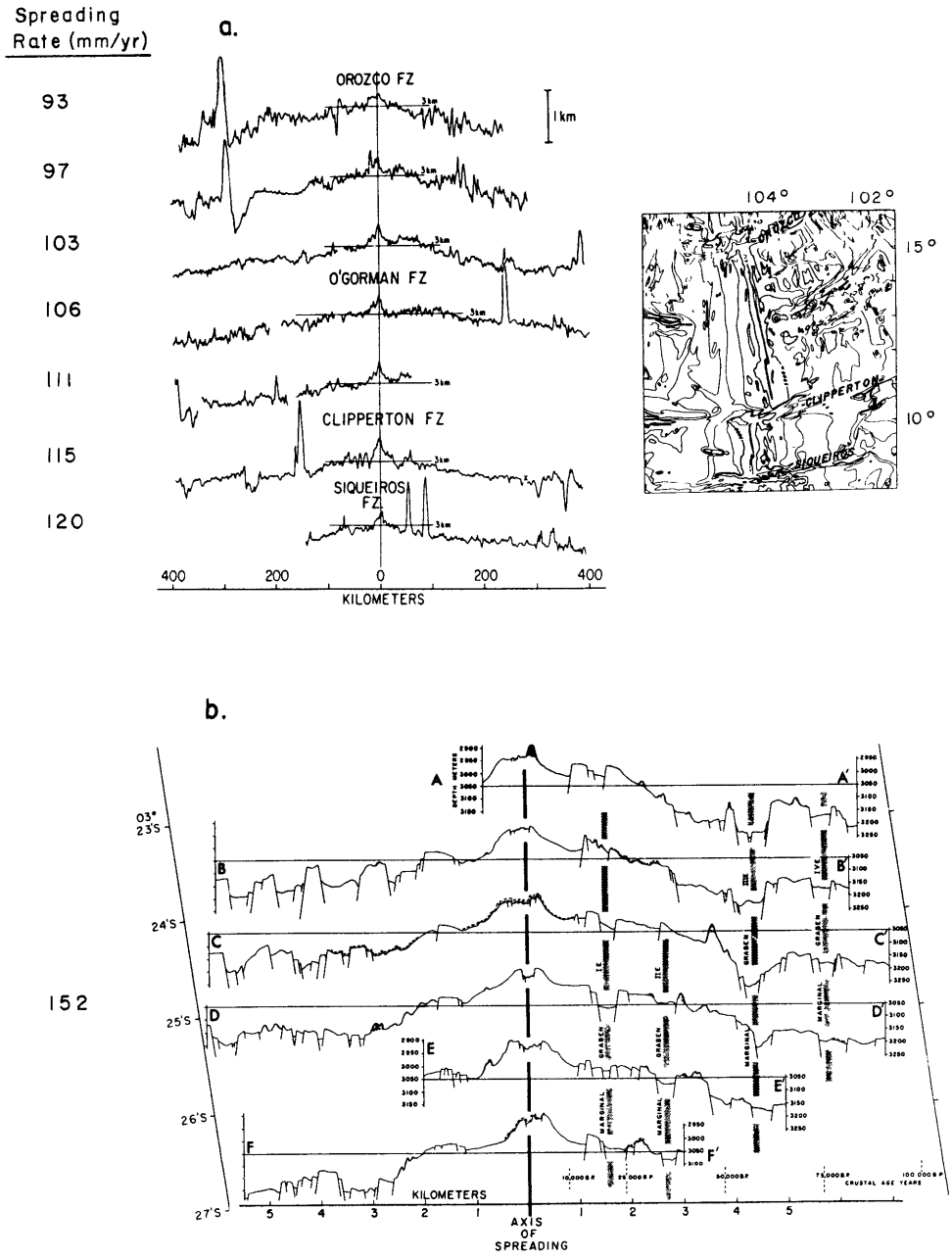

1.1 Bathymetric profiles across the East Pacific Rise with corresponding spreading rates (total) at left. a) Broad swell associated with the mid-ocean ridge is shown as well as the narrow axial high (above 3000 m). Profiles were taken from Klitgord and Mammerickx (1982) and have been compiled from several tracklines in the regions indicated. The locations of the major fracture zones, between which the compiled profiles are drawn, are shown on the 500 m contour interval map at right (revised from Klitgord and Mammerickx (1982) to include axial bathymetry from Macdonald et al. (1984)). b) Ridge morhpology near 3°25'S taken from Lonsdale (1977b). Profiles are oriented perpendicular to the ridge axis. Latitudes of the 3050 m lines are indicated by the bounding tick marks which are labeled on the left.

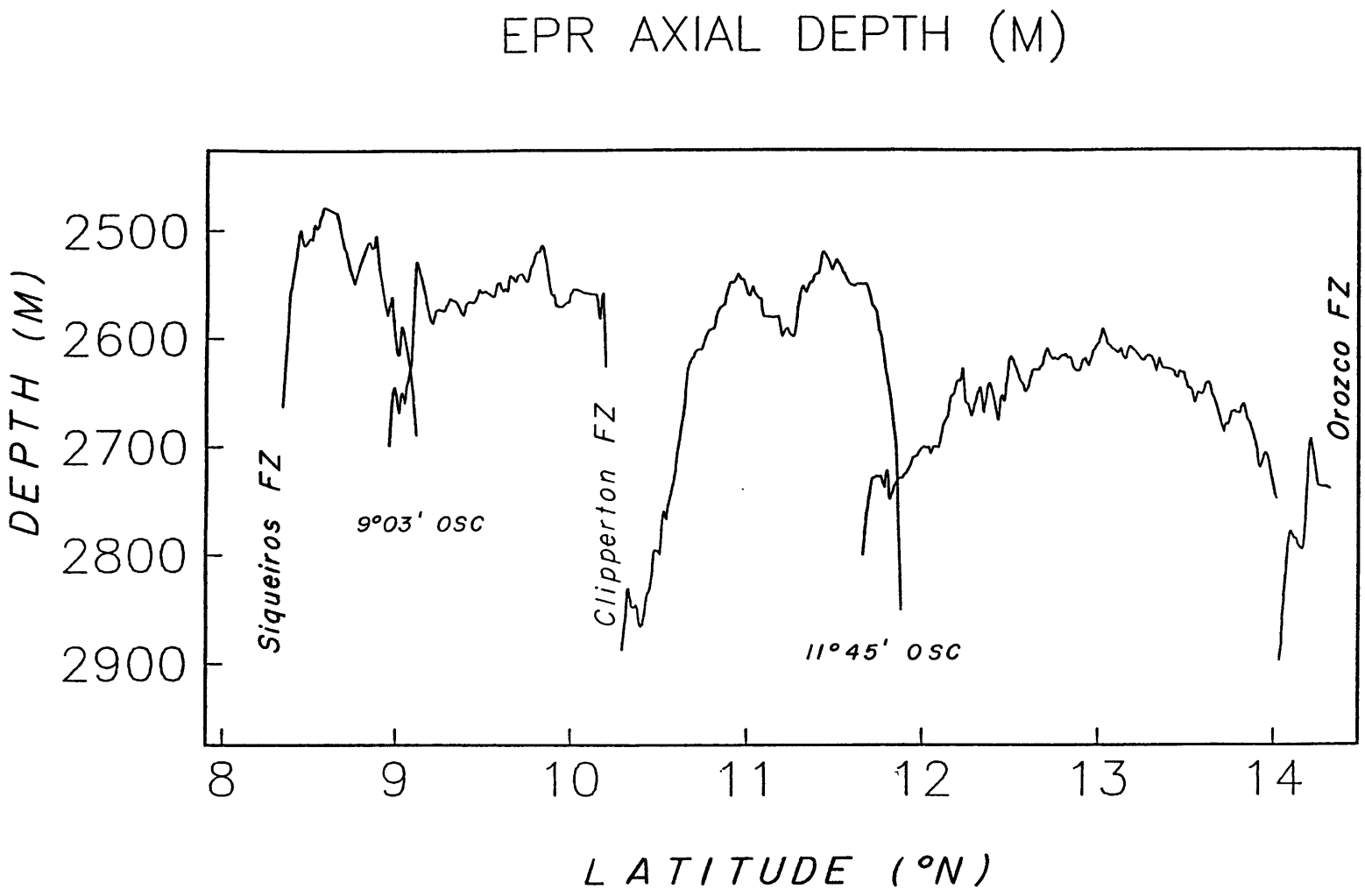

1.2 Along-strike axial depth profile of East Pacific Rise segments projected onto a single plane. Ridge discontinuities at fracture zones and large offset OSCs are labeled.

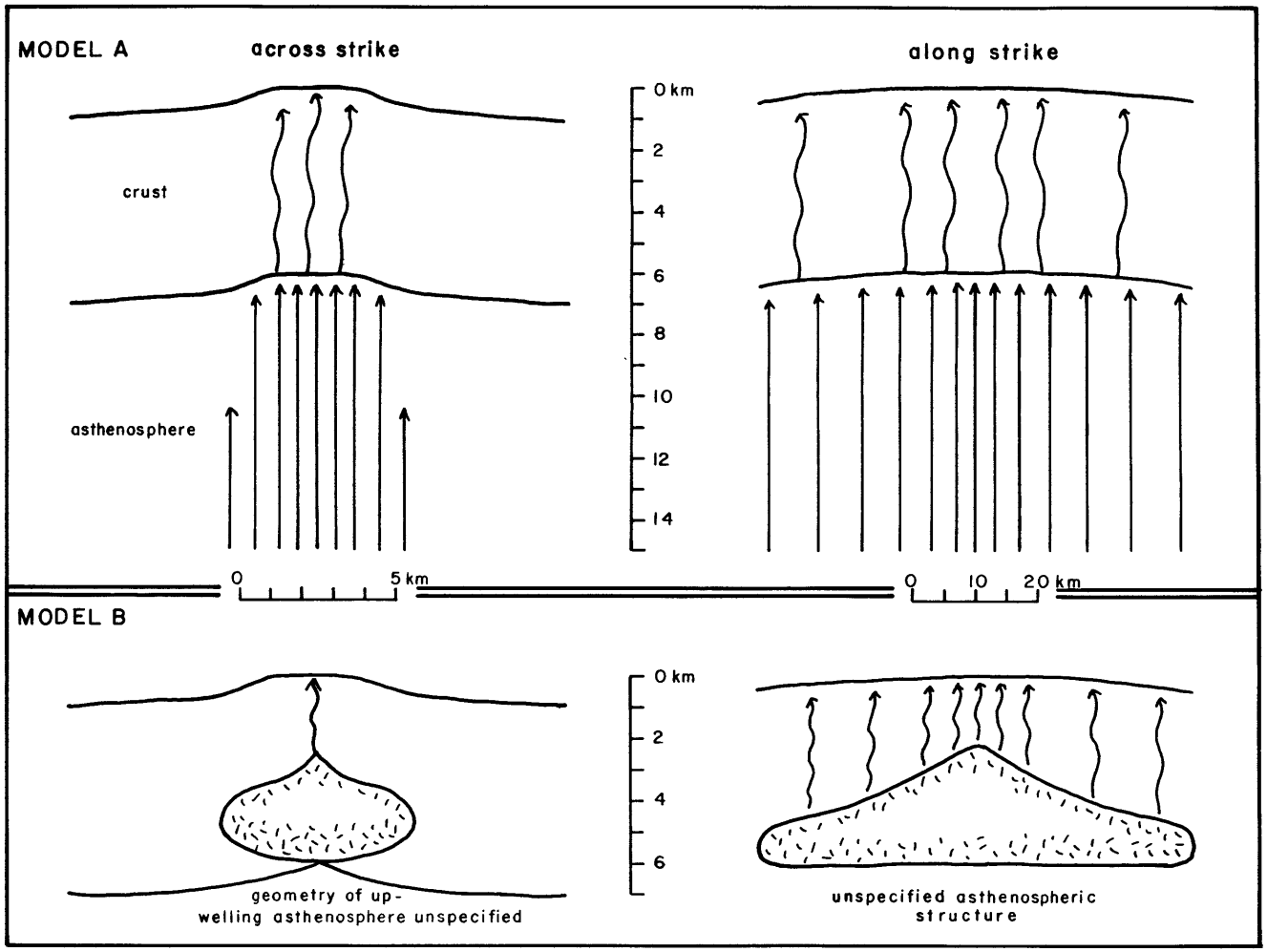

1.3 Two end member models that form the basis for isostatic modeling of axial density structure. Model A emphasizes the subcrustal melt distribution and length of arrows schematically indicates flow velocity of melt. Model B emphasizes melt in a crustal magma chamber. Crystallization is indicated along the walls, ceiling and floor of chamber by hachures. Cross-sectional structure of each model is depicted on left with no vertical exaggeration. Along-strike structure of a single ridge segment is depicted on right, VE = 5:1.

2. Observational Data

The general morphology of a fast spreading mid-ocean ridge consists of a 2-15 km wide axial ridge which stands 200-400 m above the broad swell, as described in the previous section. The purpose in this section is to point out the character of the ridge segments that terminate at overlapping spreading centers, noting the topographic and geologic changes along-axis as well as structural inferences drawn from geophysical data. The SEABEAM data that form the observational base for this study have been published only within the last few years (Macdonald and Fox, 1983; Lonsdale, 1983, 1985; Macdonald et al., 1984). At this time several theories have been put forth to explain the structure and proposed evolution of OSCs. Here the combined SEABEAM coverage, further analysis of these data and recent petrologic data are reconsidered together, rather than separately as has been the case in earlier studies.

Brief review of previous observations An example of two ridge segments that are offset at an OSC and the terminology that will be used in discussing the system is shown in Figure 2.1. The ridge segments overlap and curve towards each other around the overlap basin. The segments vary, over a distance of a few kilometers, from broad to narrow and from shallow to deep. There is no consistent relation between the width of ridge and its position in the OSC system but there is an obvious correspondence of ridge height and position, the deepest parts occurring near the offsets (Francheteau and Ballard, 1983; Lonsdale, 1983; Macdonald et al., 1984). The two ridge segments overlap morphologically for a distance of 20-30 km but it is uncertain whether

or not significant magmatic activity or spreading occurs at both ridges during a single time period. Hekinian et al. (1985) cite submersible and SEAMARC I data as evidence that activity is presently occurring on only the western ridge segment at the (left stepping offset) 12°53'N OSC. Yet, this is one of the smaller OSCs and therefore may not be representative of the large OSCs. Sempere and Macdonald (in press) report evidence of some relatively fresh material at both the eastern and western ridges between 9°00' and 9°05' at the 9°03'N OSC.

Previous studies tend to treat all OSCs as similar structures which may be an oversimplification. If all OSCs developed and evolved by the same mechanisms, the complete range from small offset to large offset should be observed. Instead, the distribution of OSC offset is almost bimodal for the EPR (Figure 2.2) with 1-2 km offsets in one group and 8-12 km offsets in another group. The smaller offset OSCs are associated with axial depth anomalies of 50 m or less (compared to about 200 m at large offset OSCs) and they are often contained within the general ridge structure rather than being distinct ridges separated by an overlap basin. In order to avoid complication due to what might be two similar yet unrelated (in terms the processes controlling the morphology and its evolution), only larger offset (7-12 km) OSCs will be considered in detail here.

Five large OSCs have been recognized along the EPR, four (not including the 3°24'N OSC (Lonsdale, 1985)) have been surveyed fairly completely and comprise the basis for this study. The 11°45'N and 9°03'N OSCs were first recognized by Macdonald et al. (1984), the 5°30'N by Lonsdale (1985) and the 5°30'S by Lonsdale (1983). Figure 2.3 is

compiled from figures taken either directly from or slightly modified from these publications. Viewed together, the four OSCs are seen to have several features in common: all are offset in a right stepping sense; all have steeper sided ridge flanks on the overlap basin side compared with the other side; all have one broad tip and one shallow, narrower tip; all are strikingly similar in their geometry and scale of offset and overlap. The relief is greater at the 5°30'N and 5°30'S OSCs with the maximum depth of the overlap basin surpassing the general off-axis depths by 200 to 300 m. At the 9°03'N and 11°45'N OSCs the basin depth is approximately the same as the depths of the topography 5 km off-axis. The shapes of the two overlapping ridges are different and more exaggerated at the 5°30'N and 5°30'S OSCs than at the others. The 11°45'N, 9°03'N and 5°30'S OSCs have a broader eastern ridge tip than western whereas the 5°30'N has a broader western tip. The narrow ridge tip at both the 5°30'N and 5°30'S OSCs is quite steep and triangular compared with 11°45' and 9°03'N.

Cross-sectional profiles of the four OSCs, drawn every nautical mile along-axis, are shown in Figure 2.4. For each of the four OSCs a line paralleling the general EPR axial trend was drawn through the center of the overlap basin. Profiles perpendicular to this centerline were digitized from the 20 m contour interval maps shown in Figure 2.3. The digitized points were fit by a cubic spline which was then checked for consistency with the original map. Along most profiles there is complete SEABEAM coverage, but there are some areas that have been interpolated between tracks crossed by a given profile or between the SEABEAM data and conventional bathymetry data outside the OSC (see the

inset maps in Figure 2.4).

The axial ridge in Figure 2.4 has been shaded above the depth where corresponding regional bathymetric profiles have been shown to fit the $\sqrt{t}$ cooling curve (Klitgord and Mammerickx, 1982; Lonsdale, 1977). This reference depth varies along the EPR so that it is about 3000 m deep at 11°45'N, 2900 m at 9°03'N, 3100 m at 5°30'N and 3000 m at 5°30'S. The reference depth at any one OSC could be shifted by ± 50 m since the regional bathymetric profiles are not available at each of these areas precisely. The reference values listed above are used since they depict the eastern and western ridges similarly at all four OSCs.

Along-axis profiles of the minimum axial depths projected onto a plane through the center of the OSC are shown in Figure 2.5. Note the broad ridge segment highs between major offsets (Francheteau and Ballard, 1983; Crane, 1985) upon which are superimposed local highs. The axial depths increase steeply at the ridge tip, dropping off at 10-30 m/km compared with a slope of 1-3 m/km in the center of the segment (Lonsdale, 1983; Macdonald et al., 1984).

Magnetic data have been collected over the 9°03'N and 5°30'S OSCs (Sempere et al., 1984; Lonsdale, 1983). Sempere et al. (1984) show that a magnetic high is associated with the eastern ridge tip of the 9°03'N OSC. They fit the anomaly with a body of high magnetization beneath the tip which is inferred to be composed of Fe-Ti rich basalts. Based on reports that Fe-Ti basalts are found at the Galapagos Propagating Rift tip (Sinton et al., 1983), Sempere et al. (1984) infer from the magnetic inversion at 9°03'N that the eastern ridge segment is propagating to the south. Lonsdale (1983) interprets a magnetic trough, mapped from widely

spaced tracks on the ridge flanks 40 km to each side of the 5°30'S OSC, as evidence that the creation of highly magnetized crust has persisted through time at this part of the EPR. He suggests that anomalous crust created at the ridges where they overlap is more highly magnetized than typical crust and is responsible for the anomaly.

Deep Tow and submersible data reported by Thompson et al. (1985) and Sempere and Macdonald (in press) indicate that the western ridge tips of the 11°45' and 9°03'N OSCs are presently inactive, tectonism and sedimentation being greater there than at the mid-segment highs to the south . These authors show that the overlap basin is apparently a passive structure with little tectonic fabric or sign of recent activity. In contrast, they show that the eastern ridge tips at these two OSCs have been quite recently active, volcanism occurring within narrow fissure zones contained in the broader tip high.

Dredge samples collected by Thompson et al. (1985) from the western mid-segment high, a location near the western ridge tip and one near the eastern ridge tip of the 11°45'N OSC have distinct petrologic signatures. Basalt compositions along the western segment can be explained by fractional crystallization of a single, assumed to be centrally supplied, magma batch. The eastern ridge samples are quite different, more evolved and interpreted to result from propagation of this ridge to the south into older crust. Also, Langmuir et al. (submitted) report that basaltic glasses from the eastern ridge segments north of the 9°03' and 5°30'N OSCs are more silicic than those found elsewhere along the segments, yet similar to those found at propagating rifts.

The data reviewed above form the observational framework that constrains the analyses in the following sections, the first of which presents an attempt to estimate the volume of the axial ridge along the EPR, in general, and its variation at OSCs.

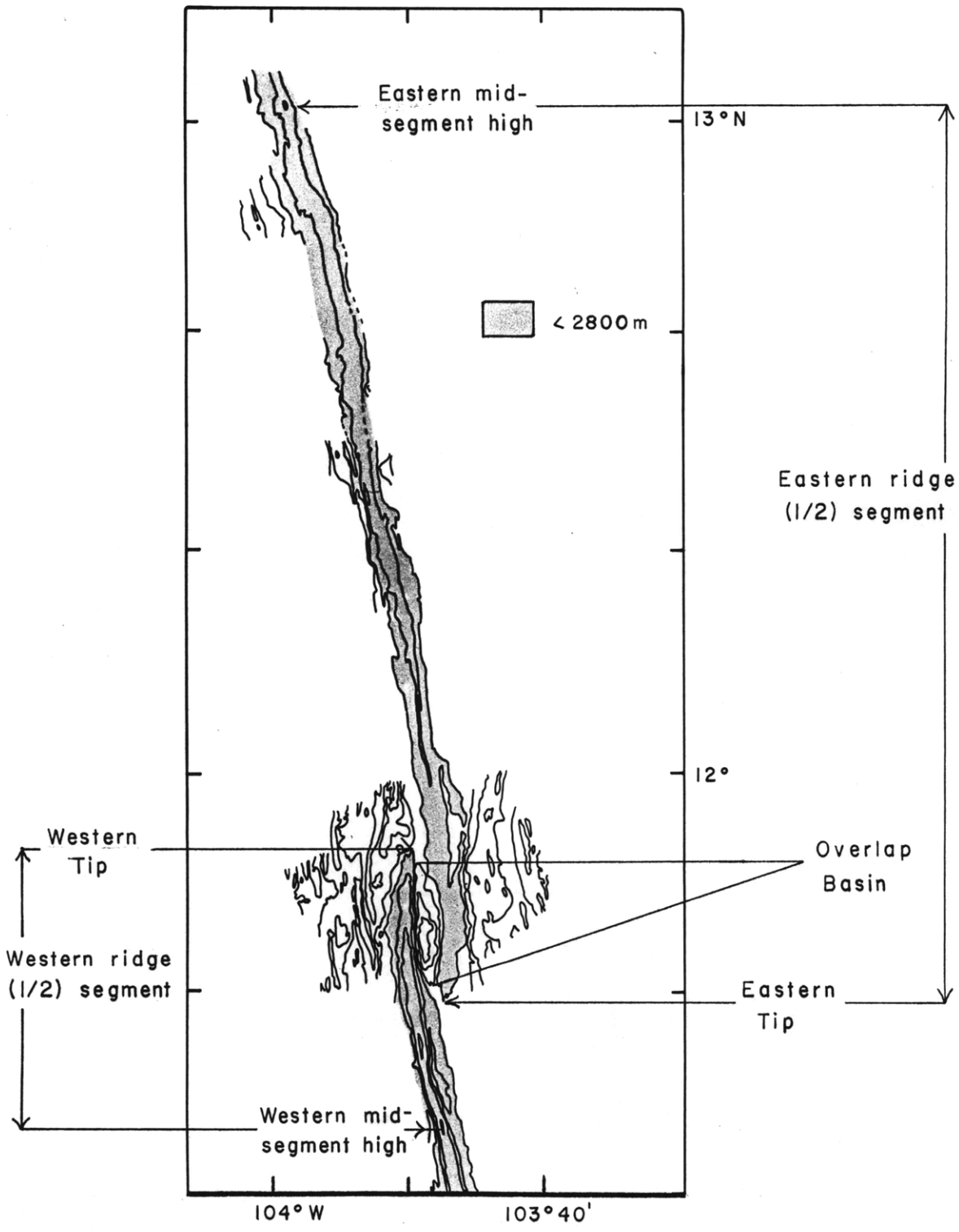

2.1 Bathymetric map of eastern and western ridges and their termination at 11°45'N OSC. Terminology for various parts of OSC system are labeled. Contour interval is 100 m, depths less than 2800 m are shaded to highlight ridge axis. Contours taken from Macdonald et al. (1984).

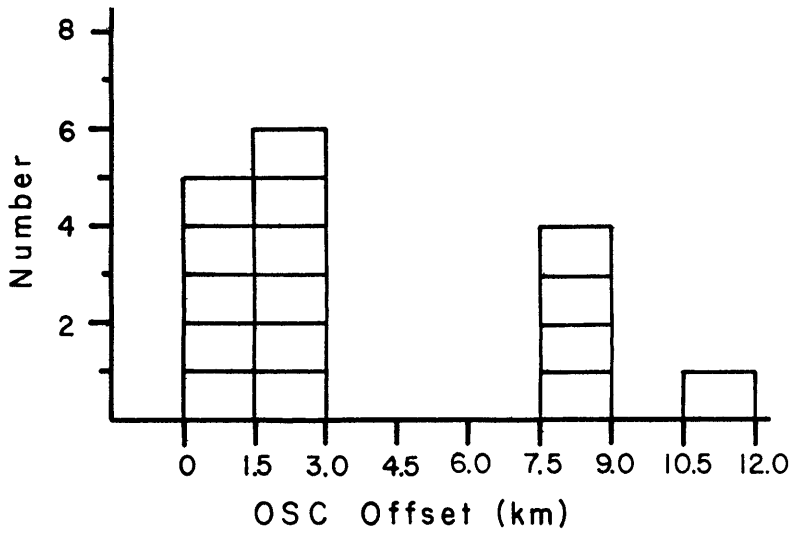

2.2 Histogram showing number of EPR OSCs of a given offset. 16 OSCs from Lonsdale (1983, 1985) and Macdonald et al. (1984) were considered.

5°30'S OSC

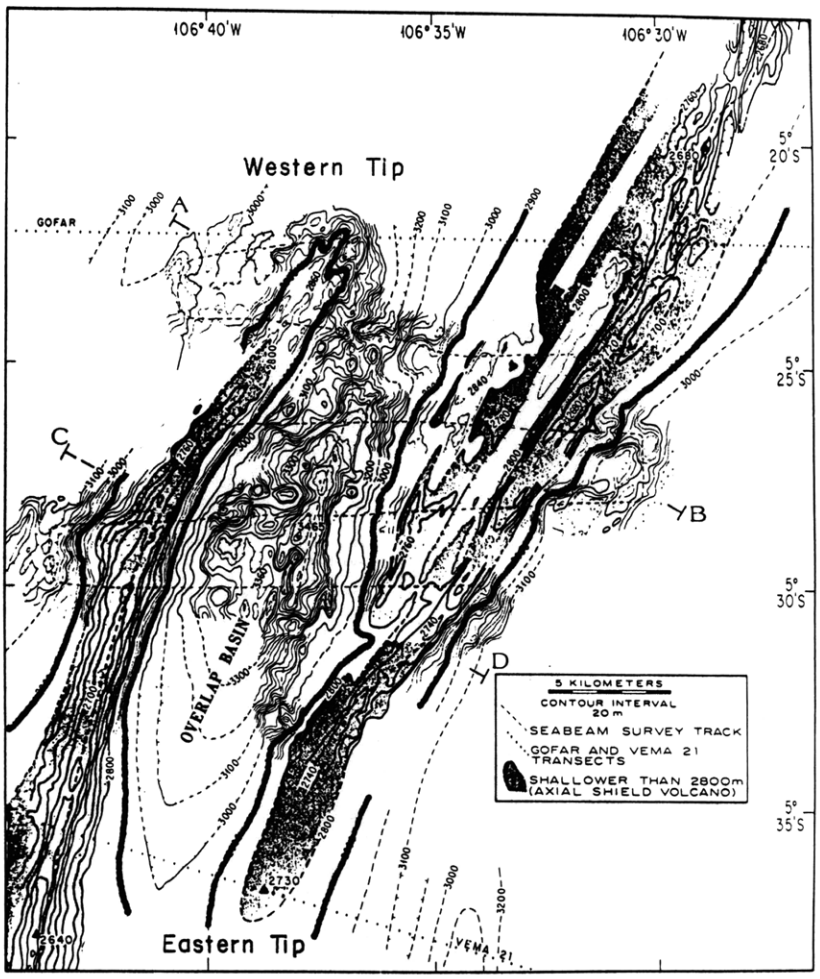

2.3a

2.3 a-d) Maps of SEABEAM data for four large offset OSCs along the EPR. Contour interval is 20 m. Heavy line indicates depth 100 m less than regional off-axis depth and is intended simply to delineate the ridge axes for the varying map styles. 2.3a taken from Lonsdale (1983); 2.3b from Lonsdale (1985); 2.3c and 2.3d from Macdonald et al. (1984).

5°30'N OSC

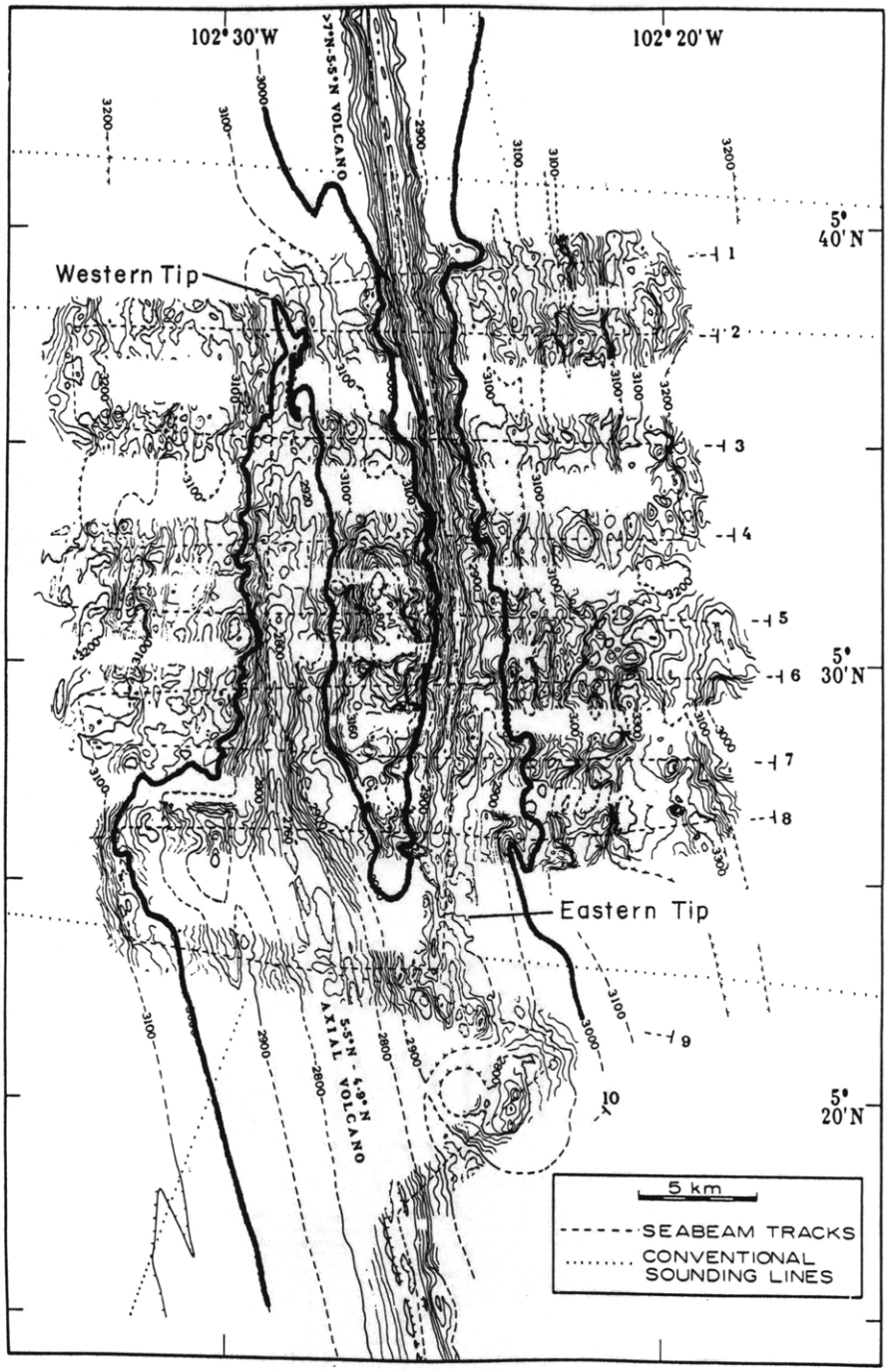
102° 30'W
102° 20'W
5° 40'N
5° 30'N
5° 20'N
Western Tip
Eastern Tip
7°N-5.5°N VOLCANO
5.5°N - 4.9°N AXIAL VOLCANO
11
12
13
14
15
16
17
18
19
10
5 km
SEABEAM TRACKS
CONVENTIONAL SOUNDING LINES

2.3b

9°03'N OSC

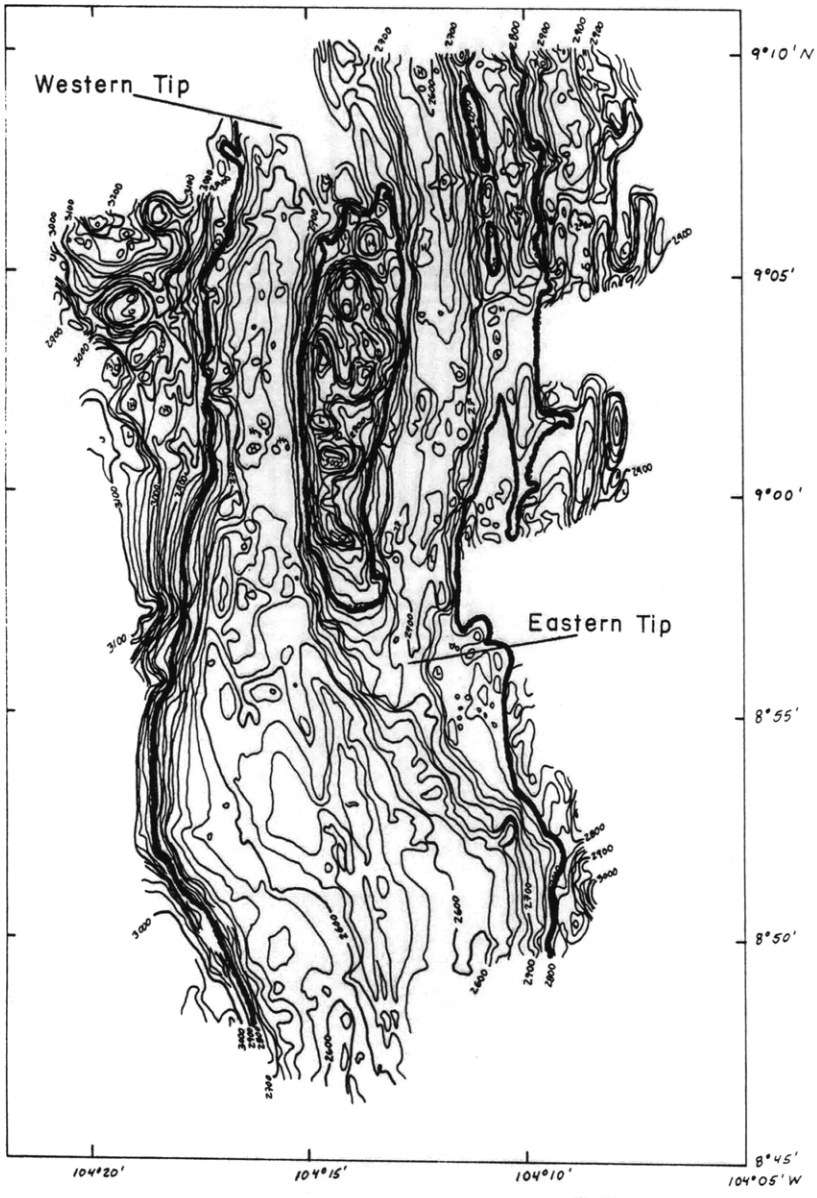
Western Tip
Eastern Tip
9°10'N
9°05'
9°00'
8°55'
8°50'
8°45'
104°20'
104°15'
104°10'
104°05'W

2.3c

11°45'N OSC

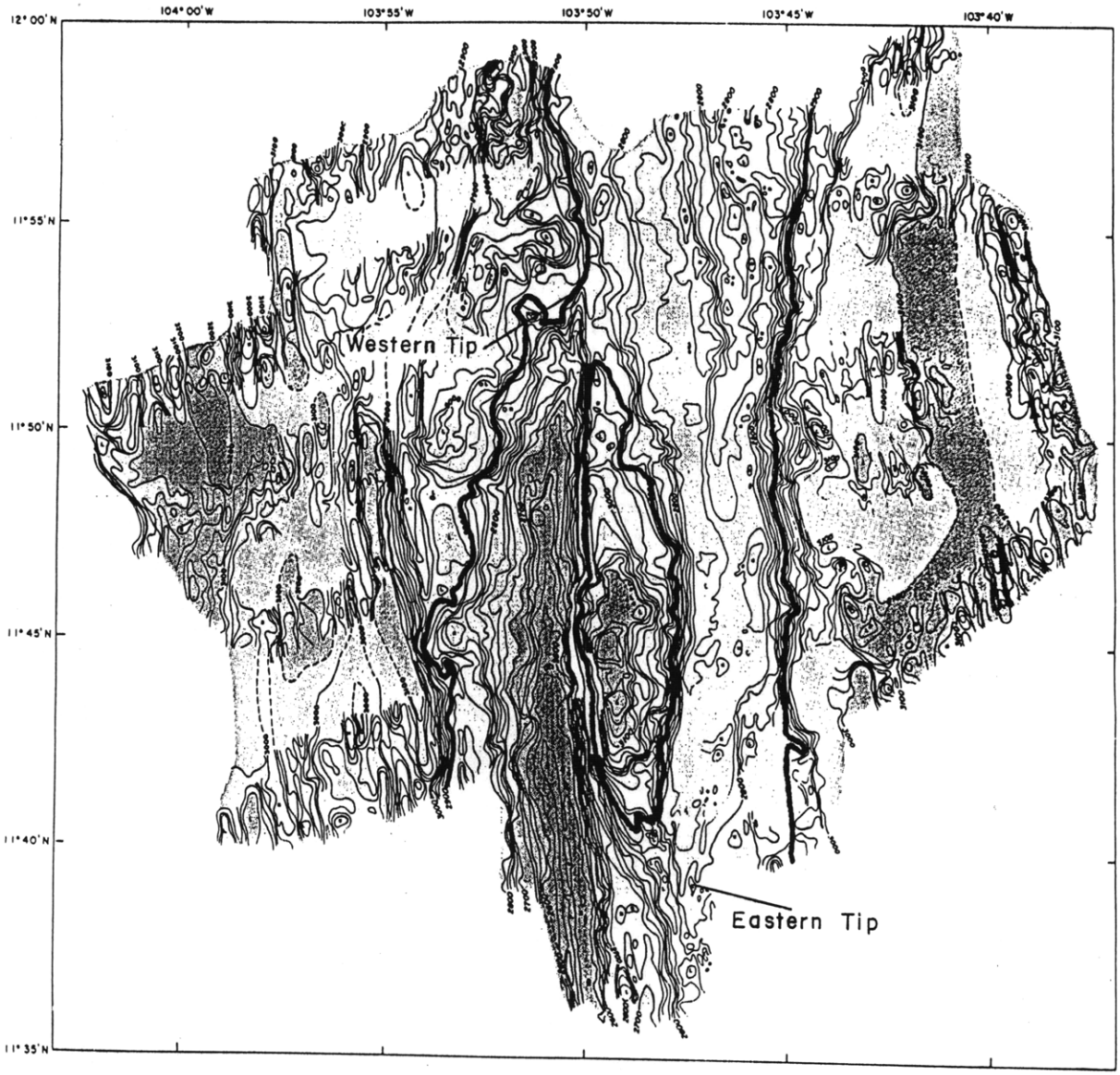

2.3d

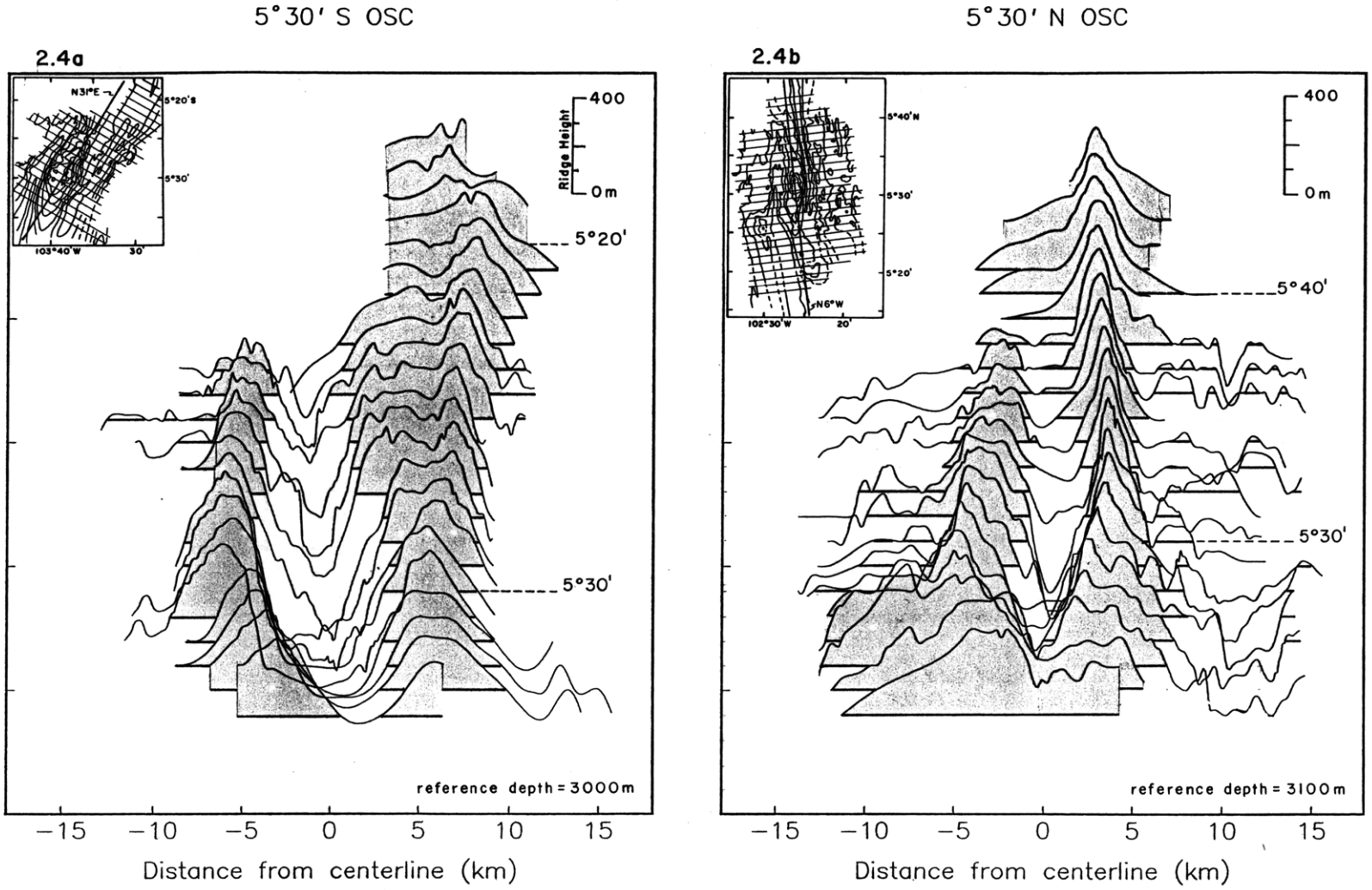

2.4 a-d) Cross-sectional bathymetric profiles in series, spaced 1 nautical mile apart, for large offset OSCs. Inset maps show orientation of centerline (approximately parallel to trend of axis) and perpendicular profile lines. Ridge axes are shaded above the reference depth which is listed at the lower right of each frame.

9°03'N OSC

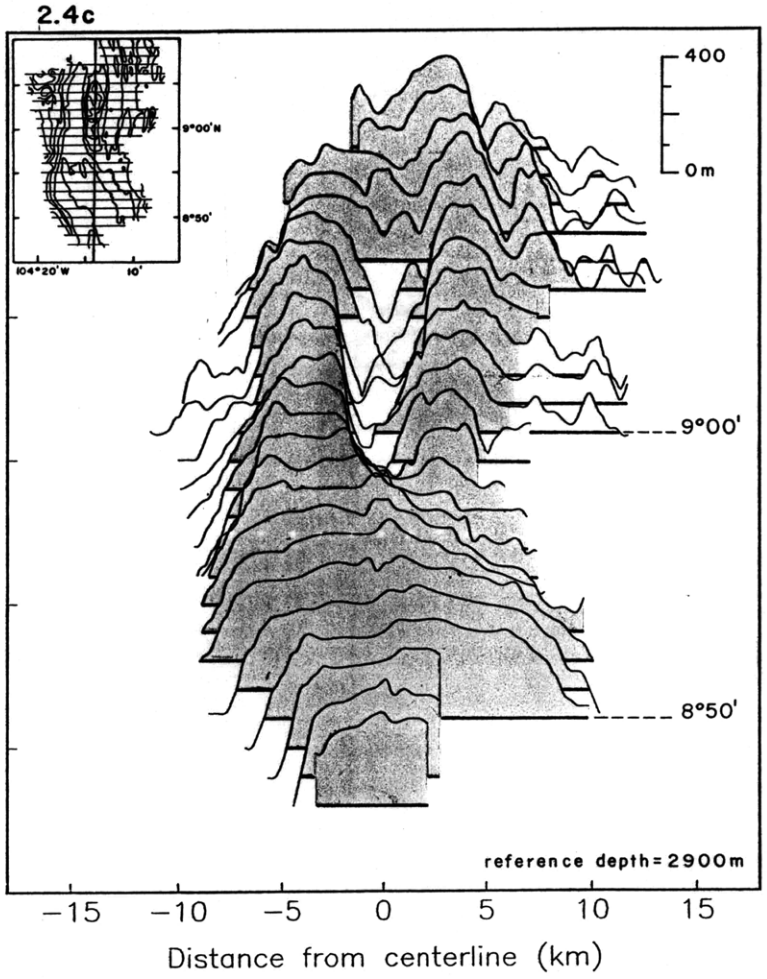

11°45' N OSC

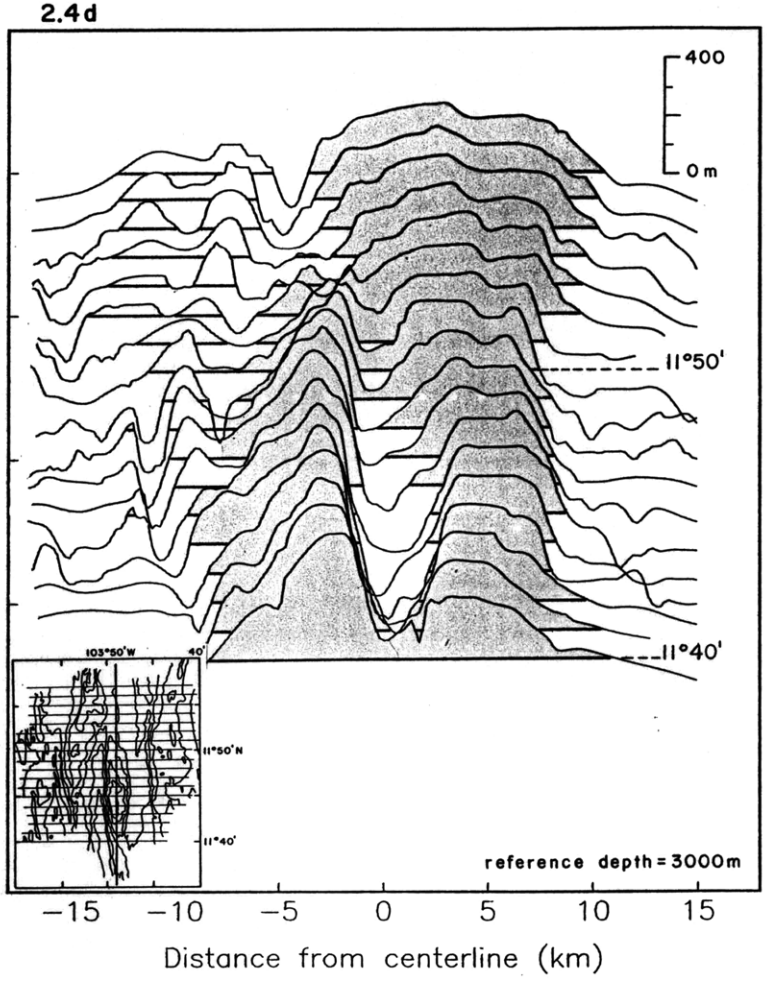

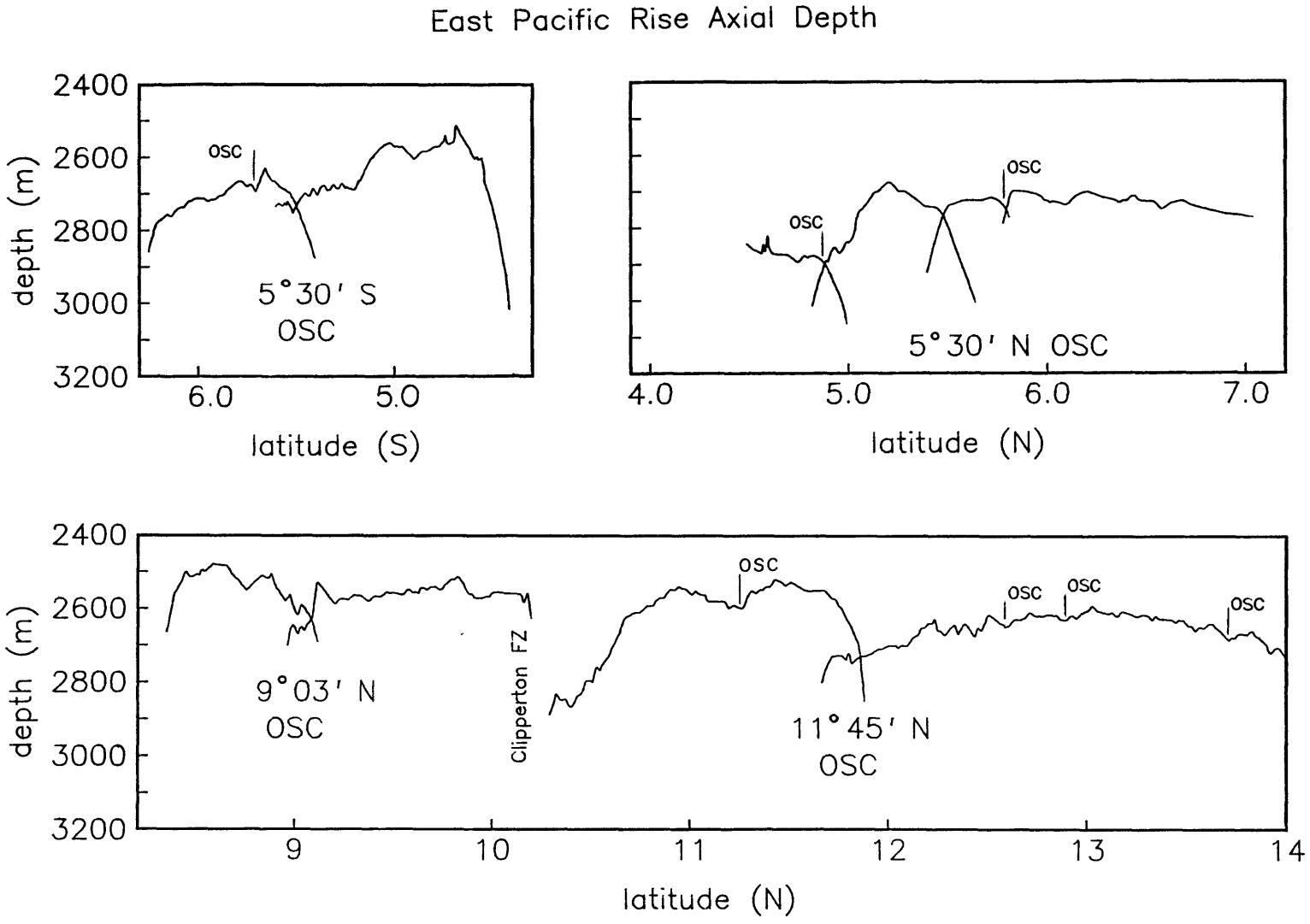

2.5 Axial depth profiles, projected onto a plane, for ridge segments that terminate at large offset OSCs. Small offset (1-2 km) OSCs are labeled above, large - below. Profiles digitized from Lonsdale (1983, 1985) and Macdonald et al (1984). VE ≈ 200X.

3. Axial Ridge Volume

Methods. The volume of the axial ridge is computed, for one meter thick sections, by taking cross-sectional profiles and determining the area above a reference depth (the depth predicted by the $\sqrt{t}$ cooling curve). At the large OSCs the axial volume corresponds to the shaded areas in Figure 2.4. Elsewhere, smaller SEABEAM surveys (13°N, Francheteau and Ballard, 1983) and wide-beam echo sounding profiles (6° and 10° S, Rea, 1975; 1976) can be used to determine ridge volume. SEABEAM coverage to the north and south of the 11°45'N OSC (Macdonald et al., 1984) includes enough of the axis that it is possible to estimate the volume along the ridge from the mid-segment highs to the tips, but a somewhat involved method is necessary.

The axial SEABEAM data to the north and south of the 11°45'N OSC does not include enough of the ridge flank to reach the reference depth, in general, but there are two places where the coverage extends out to 10 km. At 12°50'N there is data to the west of the axis and at 13°10'N there is data to the east. By combining profiles, one from each of these areas, a representative 'flank profile' was formed. This flank profile was then used to 'complete' axial profiles that were digitized every nautical mile (11°25'-13°02') from Macdonald et al.'s (1984) 20 m contour maps. The method used to attach the flank profile to the axial profile is illustrated in Figure 3.1 and was as follows: the axial profile for a given latitude was centered within the flank profile; the depths of the end points (easternmost and westernmost) of the axial profile were compared with the depths of the flank profile at the same distance from the axis; if the depth of the flank profile was greater

than or equal to that of the axial profile then the profiles were attached there at the endpoint. Otherwise the first point, in the direction away from the axis, at which the flank profile depth equalled or exceeded the axial profile depth is where they were attached; the section between the endpoint of the axial profile and the point of attachment to the flank profile was connected with a linear interpolation. For all the cross-sectional profiles, the volume was estimated by multiplying the average ridge height between adjacent digitized points by the distance between the points, summing along the profile. This is only a crude estimate but with the inaccuracies introduced by using the flank profiles outside the axial region a more sophisticated method seems unwarranted.

Results. The results of the volume calculations are shown in Figure 3.2-3.5. Both the bathymetry and the volume of the 11°45'N OSC, from mid-segment high on the western ridge to mid-segment high on the eastern ridge, are shown in Figure 3.2. Most noticable is the drop in volume across the overlap region to about 30% of the average ridge volume to the south. (There is some discrepancy at the junction between the values computed using the continuous (off-axis) profiles, in the vicinity of the OSC, and those computed using the flank profile. But, for the purpose of this initial investigation no attempt has been made to alter the flank profile to force a match of the volumes and the junctions.) Variability on the scale of 10-30 km is evident, particularly along the eastern ridge which has three broad volume highs between the mid-segment high and the overlap. The two larger broad highs correspond to sections of the ridge that are offset at small OSCs.

The 'peak' of the third broad high coincides with a local bathymetric peak at 12.23°. Superimposed on the broad volume undulations are smaller amplitude, short wavelength variations, some of which correspond to topographic peaks but several of which show no clear correlation with the axial bathymetry.

Volume estimates have been made at the other three large OSCs (in the region of overlap only, as constrained by the SEABEAM coverage) as well as at a few other EPR crossings. Axial ridge volume varies along the rise from 1 to 5 X 10^6 m^3/m, with most of the segments shown falling in the 2 to 4 X 10^6 range (Figure 3.3). Each of the four OSCs has a range of total volume (east and west ridge volumes combined) greater than 7 X 10^5 m^3/m with the volume decreasing almost monotonically from south to north at all but the 5°30'S OSC. At the 11°45'N OSC the western ridge has greater volume than the eastern ridge except for the last 3 km of the tip (Figure 3.4a). In contrast, at the 5°30'N OSC both segments have about the same volume up until the last few km of each ridge tip (Figure 3.4b).

There is some correlation between ridge volume and geochemistry. Using the data of Langmuir et al. (submitted) and Thompson et al. (1985), the variation of bathymetry and ridge volume are compared to variations in Ba/TiO_2 and Sr for the eastern and western ridges of the 11°45'N OSC (Figure 3.5). Along with the previously noted increase in geochemical variability in the region of the large overlap (Langmuir et al., submitted), there is a striking correlation between the volume low at 12.42° and the sharp increase in both Ba/TiO_2 and Sr. A similar, but smaller amplitude, signal is observed at about 12.02°. In the

latter case, the Ba/TiO_2 and Sr decrease again to the north as the volume high associated with the 12.21° topographic high is reached. North of the 12.42° volume low, the geochemical variability does not drop off until the volume high associated with the small offset OSC at 12.88°. There, the Ba/TiO_2 decreases to about half, though the Sr signal is only slightly reduced.

In both of the above cases of correlation between ridge volume, bathymetry and geochemistry, the southern limit of the region of higher Ba and Sr coincides with the base of a local topographic high. In map view, at 12.02° the ridge begins to broaden to the south of this high and the crestal peak is no longer distinguishable. At 12.42°, it is dificult to point out any significant change in the map-view character of the ridge which might indicate a change in magmatic processes that is reflected in the geochemistry. Although the role of these two axial highs in general ridge processes is uncertain, it is interesting to note that, along this section of the ridge, geochemical variability does not appear to correlate as strongly with ridge offsets as it does with local, probably constructional, topography.

This initial attempt at quantifying the volume variations along-strike a MOR suggests that total axial ridge volume decreases by 30-50% at three of the four large offset OSCs and that broad volume highs correlate mainly with widening of the ridge at small offset OSCs. The volume highs associated with local axial topography along the eastern and western segments of the 11°45'N OSC are narrower than those associated with the small OSCs. The estimates obtained here are rather crude and it will certainly be necessary to check these results when

more complete off-axis coverage is obtained. The reference depths used are subject to some uncertainty and it is possible that the regional off-axis depth varies over a distance less than that between mid-segment highs. If this is the case between 11°25'N and 13°00'N, the volume estimates for these ridge segments will need to be revised. The implications of the volume variations will be discussed in the section 5. First, the range of density structures constrained by an assumed isostatically balanced ridge topography, and the melt distributions they imply, are determined in the following section.

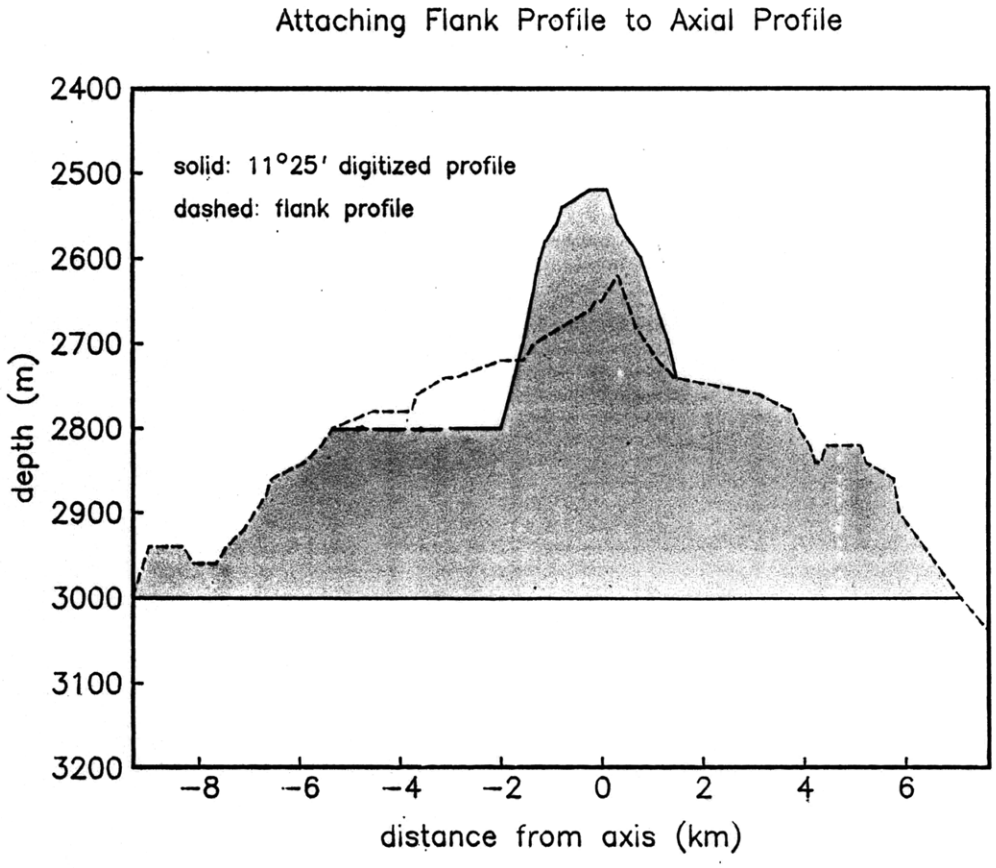

3.1 Example of 'completing' cross sectional profile by attaching flank profile to digitized axial profile (from Macdonald et al. (1984) 20 m contour maps). Axial profile is centered within flank profile. To east, axial profile is attached to flank profile at end point. To west axial profile is connected to flank profile by linear interpolation between axial end point and ≃ -6 km on flank profile. Area used to compute axial volume (shaded) is taken above reference depth.

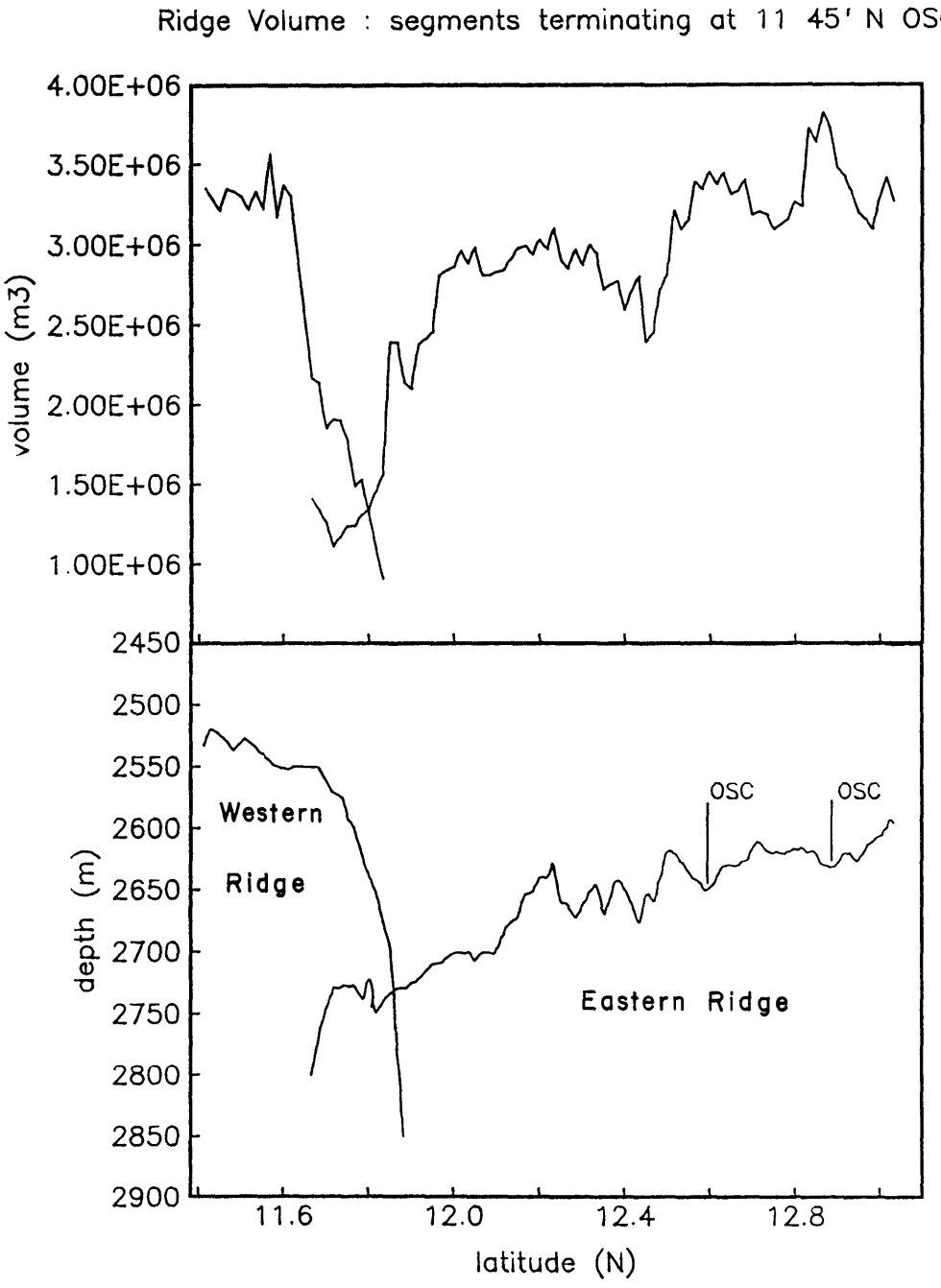

3.2 Axial volume of eastern and western ridges from mid-segment high to ridge tip at 11°45'N OSC (see text for method of determining volume). Corresponding axial bathymetry is shown below.

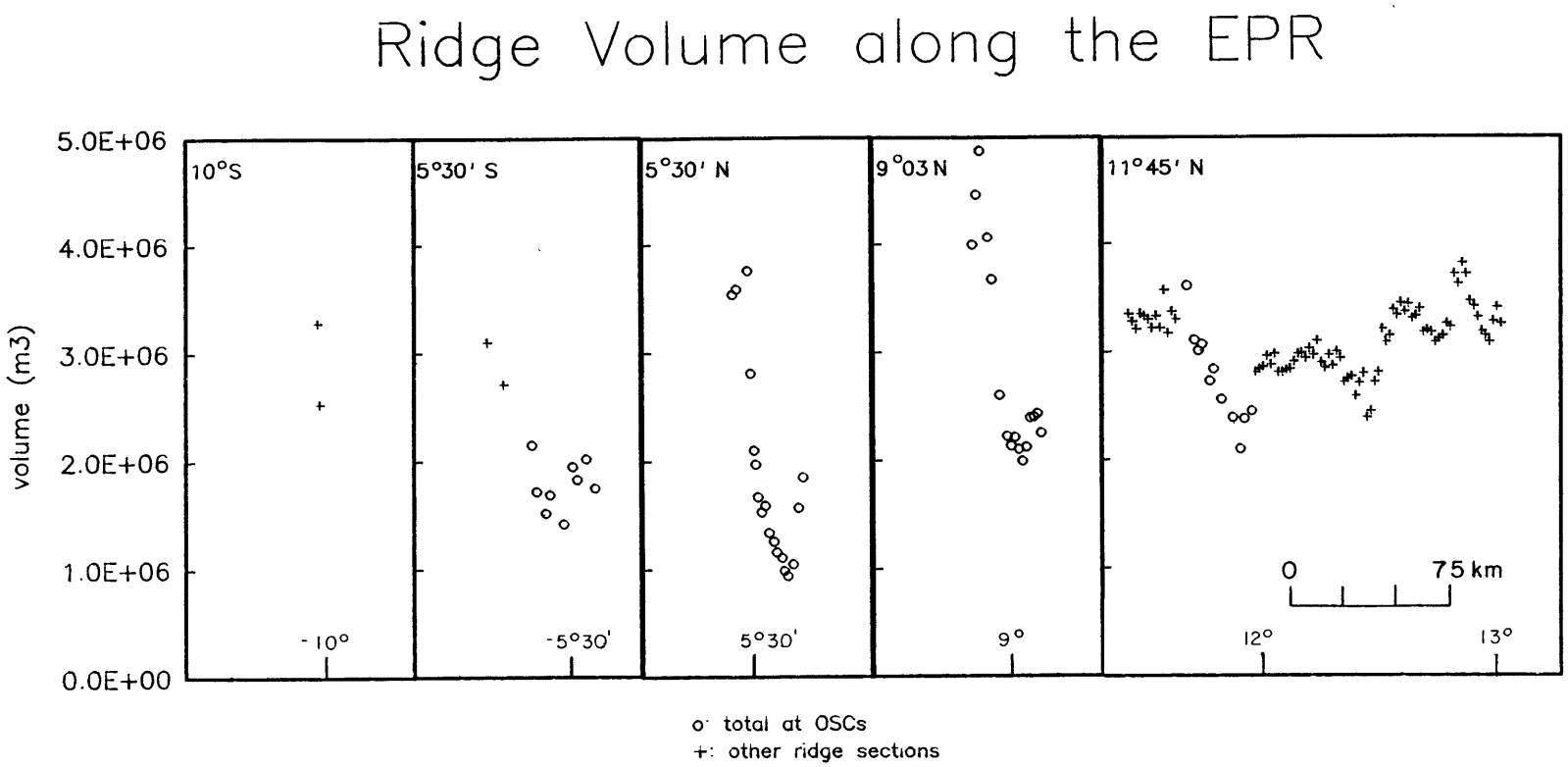

3.3 Axial volume at several locations along the EPR. Total volume of both eastern and western ridges is indicated by circles for 5°30'S, 5°30'N, 9°03'N and 11°45'N OSCs. Volume at other ridge locations is indicated by +'s.

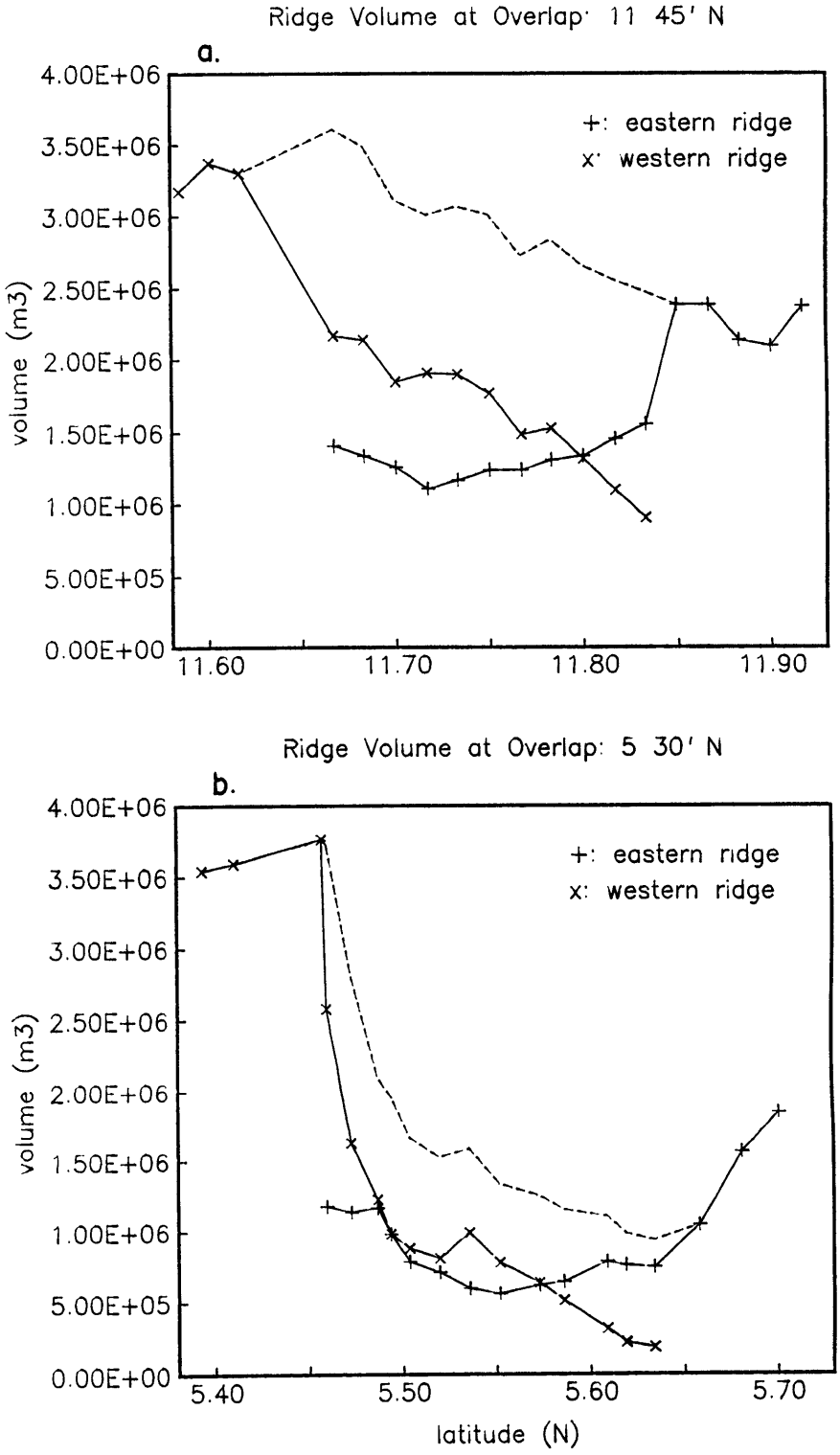

3.4 Axial volume of ridge tips at large offset OSC. Dashed line shows total volume of both ridges. a) 11°45'N OSC. b) 5°30'N OSC.

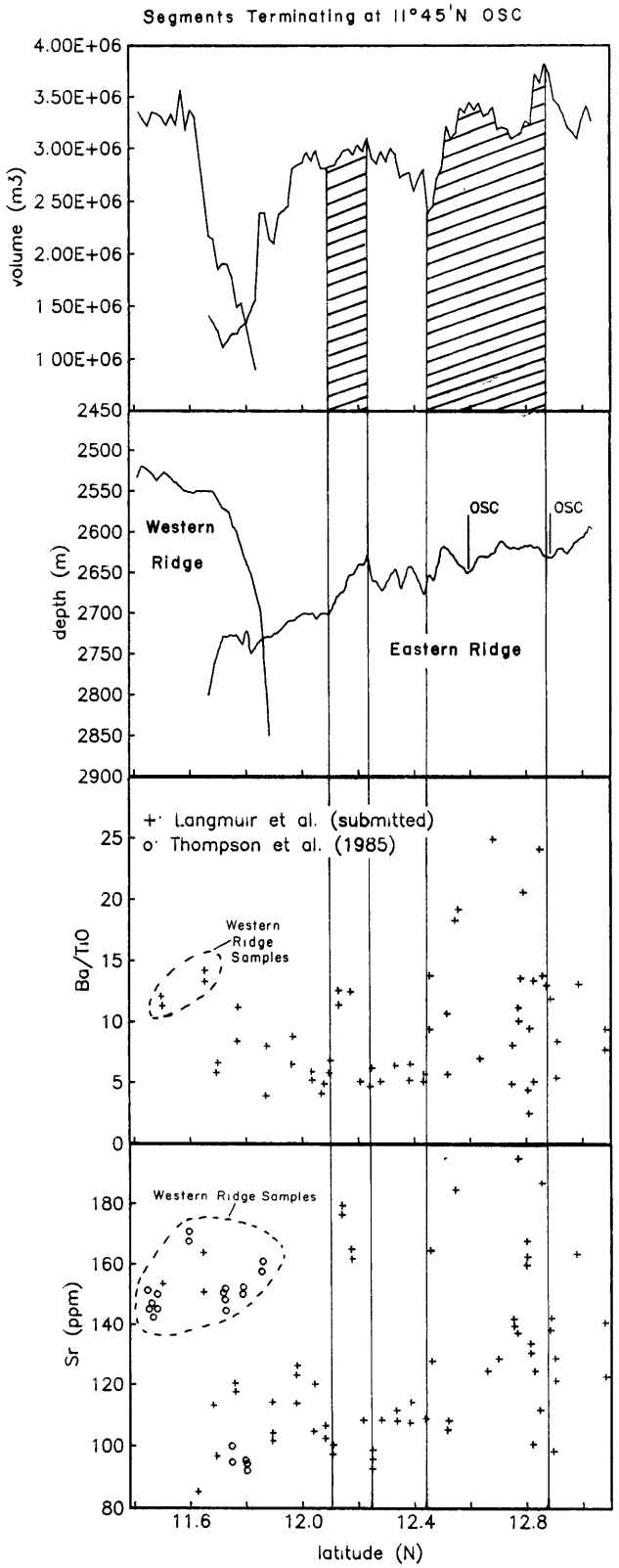

3.5 Correlation of axial volume, bathymetry and geochemistry. Shaded regions show Ba/TiO_2 and Sr highs associated with local axial topography and ridge volume.

4. Models of Ridge Density Structure

General assumptions. The intent in this section is to determine what range of plausible density structures can possibly result in the observed height of the ridge axis above the off-axis depths. I will address the problem of general ridge structure here before looking at the specific OSC structure that was covered in the previous section. It is the bathymetric variability on the scale of the ridge segments that terminate at OSCs that is of concern, though, so it should be kept in mind that the stucture under investigation is the narrow ridge axis, not the broad swell. Density structures are asssumed with the aim of realistically representing the probable ranges of effective density in the crust, asthenosphere, axial melt zone and magma chamber.

The basis for the calculations discussed below is the assumption that narrow columns in the three regions of interest (the mid-segment high, ridge tip and about 5 km off-axis) contain equal mass between the sea surface and a depth of compensation. This assumption of local (Airy) isostasy appears to be valid at and near the axis, based on gravity and thermal studies (Madsen et al., 1984; Sleep and Rosendahl, 1979; Lewis, 1981). These various authors do not agree on what depth of compensation is required to maintain an isostatically balanced ridge but Madsen, Forsyth and Detrick (1984) show that a depth just below the base of the crust is suitable at the EPR. Their model is most apropos of the system studied in this paper so a brief review of their work follows. Madsen et al. use gravity data from three sections of the EPR. Assuming a thin, broken plate buoyed from below by lower density material, they invert single symmetric profiles that result from stacking several

actual profiles within each of the three ridge sections. Their results allow a depth of compensation for the axial ridge of 4 to 10 km with values of 6-7 km preferred. They show that the gravitational and bathymetric effects predicted for a weak plate at the axis cannot be distinguished from that predicted for local isostatic conditions (ie. no component of lateral strength such as might be expected for a rigid crustal plate). Under their assumptions, subaxial negative density anomalies must be 'concentrated' within 5 km of the ridge axis and some of the anomalous mass is required to reside in the upper mantle. The model that Madsen et al. (1984) introduce, and their results showing consistency of the gravity and bathymetry data to local isostatic adjustment of the underlying density structure, will be relied upon in this study. The compensation depth is further discussed below with respect to the isostatic calculation for model A.

It should be mentioned that, although the assumption of local isostatic compensation is justified and allows the most straight forward approach to determining the effect of density structure on ridge axis height, the possibility that the ridge is dynamically supported has not yet been ruled out. Lewis (1981, 1982) has shown that gravity data can be explained by an uncompensated positive density anomaly which is supported dynamically. It is not clear that this additional complication is warranted (See Madsen et al. (1984) for a more complete discussion of the various isostatic and dynamic gravity models) and since the purpose of this study is to assess what the maximum possible contribution that a subaxial melt zone (model A) or a shallow crustal magma chamber (model B) might make to the ridge topography, it is most

useful to assume local isostasy in the vicinity of the ridge axis and, thereby, to focus on only this part of the system.

The subaxial asthenosphere model and the crustal magma chamber model are investigated separately below. The effect of varying the amount of melt present, its nonunique distribution, and the effective density contrast of the melt region (subcrustal for model A and in the magma chamber for model B) are discussed in terms of their possible contribution to the axial topography.

Subaxial asthenosphere model (A).

Methods. For this model the melt content of the asthenosphere beneath the ridge axis is the main interest. Melt contents of 3-25% might be expected in this region (eg. Bottinga and Allegre, 1973; Ahern and Turcotte, 1979). To compute the density of asthenosphere containing melt, a matrix density of 3300 kg/m^3 is assumed. For the melt a value of 2700 kg/m^3 is most appropriate for depths less than about 25 km, based on laboratory studies of basaltic melts (Kushiro, 1980; Sparks et al., 1980). At greater depths the melt probably has a higher density (up to 2900 kg/m^3; eg. Kushiro, 1980) and, therefore, the density contrast between the melt and the matrix would be less. Also, the amount of melt present at depth is lower (Bottinga and Allegre, 1978; Whitehead et al., 1984; McKenzie, 1984). Whitehead, Schouten and Dick (1984) cite peridotites bearing plagioclase as evidence that melt aggregation must occur at depths less than 25 km (above which depth plagioclase will crystallize from a melt trapped in peridotite). McKenzie (1984) shows that compaction is likely to be ubiquitous in a zone of melt migration. He shows that only about 3% melt will remain in

the matrix (solid framework component of the melting mantle) after a fairly rapid period of melt generation and extraction. The combination of a higher melt density and lower melt content results in a relatively small contribution to surface topography and gravity from the melt zone below 25 km.

In illustration of this point, consider a narrow column 10 km long, 25-35 km in depth, containing asthenosphere with 3% melt of density 2900 kg/m^3. This anomalous column contributes 36 m to the ridge height. The gravity signal of the column is negligible (modeling the column as a vertical cylinder extending from 25-35 km, with a density contrast of 12 kg/m^3 gives $g_z=9.5 \times 10^{-4}$ mgals; Telford et al., 1976). The bathymetric contribution, over 10% of the observed signal, is not insignificant but it is likely that the melt zone is not as narrow at depth as it probably is within several kilometers of the base of the axial crust. Whitehead et al., (1984) and Crane (1985) show that an asthenopsheric mush zone at depth can develop gravitational instabilities where the melt contained in the mush is channelled into localised upwellings. They, along with Schouten et al. (1985) developed the Rayleigh-Taylor instability theory to explain the regular, along-axis segmentation of ridges, but the model can also be used to suggest a means of developing a narrow upwelling region beneath a ridge axis. For the purpose of the present argument, if the subaxial melt zone is somewhat broad below the depth of melt segregation then the contribution to the excess ridge elevation from the hypothetical 10 km column is actually less than 10% since a similar column about 5 km from the axis will also contain a few percent melt. The calculated

topographic contribution of 36 m was based on a zero melt 'off-axis' (at depth) asthenosphere. Therefore, only the region above 25 km will be directly considered in this study. Although a small amount of melt is almost certainly present in the region greater than 25 km below the ridge axis, the strict definition of compensation depth as that level below which asthenosphere is uniform is not warranted in view of the small contribution to the surface signal from this region.

Results. If the crust is assumed to be of constant thickness and density, on and off-axis, then only variations in the melt content of the subaxial material will influence the ridge height. In order to achieve a mass balance of the columns it is necessary to adjust the depth of compensation to achieve the necessary ridge elevation for different melt zone densities. Assuming a 6 km thick crust, the relation between ridge height, compensation depth and melt content is shown in Figure 4.1. For 25% melt in the region extending from the base of the axial crust to about 12 km depth, a 400 m ridge can be maintained. A ridge of 300 m can be supported by a similar zone of 15% melt. In general, higher ridges require either a greater compensation depth, greater melt content, or both. The melt percents are an average over the thickness assumed (as well as over time) and therefore do not necessarily imply that a given melt percent prevails throughout the column. In Figure 4.2, several possible melt distributions are shown for 15% and 25% average melt contents.

From Figure 4.1 the decrease in subaxial melt content that would correspond to the observed along-axis deepening of the ridge can be determined. The compensation depth is constant for a given model but

the melt content decreases a few percent for each 100 m decrease in ridge height. These values will be discussed further in the next section with respect to their petrologic implications at ridge tips.

Thus far it has been shown that a narrow asthenospheric melt zone can support an axial ridge of the observed height, assuming a constant thickness crust. A more realistic model is one with thinner crust at the axis relative to off axis (Figure 4.3). The assumption of a thinner axial crust is geologically more reasonable than that of a constant thickness crust for two reasons: 1) the melt material impinging at the axis is of higher temperature than the mantle at the base of the crust off-axis therefore the depth to which material solidifies to form crust is less; 2) ophiolite models suggest that cumulate rocks form at the ridge axis and subside due to loading of subsequently formed cumulates as they spread away from the axis thereby creating a thicker crust (Cann, 1974). Since the purpose here is to explore the effect of a subaxial melt zone on the ridge topography it is assumed that the cumulate forming region just mentioned is thin and does not maintain large amounts of pure melt.

Intuitively, it is clear that a greater compensation depth will be needed to support a ridge that has a thinner axial crust than would be needed to support one with a constant thickness crust. This is because the melt material has a positive density contrast with the crust so a greater total amount of melt is necessary to achieve the same mass deficiency beneath the ridge. Figure 4.4 shows that the compensation depths are greater than for a constant thickness crust (for a given melt contrast) and they increase more rapidly with decresed melt content.

Plotted values were calculated for axial crust ranging from 1.5 to 6.0 km thickness (the latter representing constant thickness) using melt contents of 25% and 15% (Figure 4.4b). The compensation depths necessary to support a 300 m high ridge are rather large for axial crust thicknesses less than about 3.0 km and melt contents less than 25%.

It has been shown that a simple model of subaxial asthenospheric melt can explain the observed ridge elevations for fairly high melt contents and compensation depths somewhat greater than those determined by Madsen et al. (1984) from gravity data. A further contribution to the ridge height, consistent with this model, could be a mass deficiency in the axial crust due to fracturing and alteration associated with hydrothermal activity. If the effective density of the axial extrusives is significantly lowered by a dense network of fractures, as is postulated to exist for models of hydrothermal circulation, then the density contrast of this shallow region may be as important in maintaining ridge topography as the contrast in the asthenosphere.

Crustal magma chamber model.

Methods. For this model a compensation depth of 6 km, at the base of the crust, is assumed. By taking such a shallow compensation depth, one effectively assumes that the melt that is generated and segregated in the asthenosphere is not retained there in quantities sufficient to maintain a large density contrast with the surrounding material. A crustal magma chamber containing only melt (100% basaltic liquid) is assumed to exist below the axis and its thickness is varied. The magma chamber, of constant density, is assumed to thin along axis towards the ridge tip and is assumed not to be present at all in the off-axis

column. The crustal density represents an average of the density of an upper layer of basalt (Layer 2) and a lower gabbroic layer (Layer 3). An average density may represent a number of crustal configurations in terms of the thickness and densities of the upper and lower units. In Figure 4.5 possible configurations are shown for assumed average crustal densities of 2900-3050 kg/m^3. A density of 2800 kg/m^3 is used for the basaltic layer based on the density of quenched glass in laboratory studies (Kushiro, 1980). A range of 2950-3120 kg/m^3 is reasonable for the lower crust and allows for up to 1 km effective thickness of a dunite component (ρ=3400 kg/m^3).

Results. The height of the ridge that can be supported by a magma chamber depends on the thickness of the chamber and its density contrast with the surrounding crust. Since the melt density is assumed to be constant, different density contrasts reflect different choices of assumed crustal density. Figure 4.6 shows the linear dependence of ridge height on chamber thickness for various density contrasts. Both cross-strike and along-strike structures can be determined from this graph. For a given chamber thickness and $\Delta\rho$, the height of the ridge above the off-axis depth can be determined directly. The along-strike decrease in chamber thickness necessary to support a ridge of decreasing height can be determined by finding the thickness for the height of the mid-segment high and subtracting the thickness for the height of the tip. For example, the 3.83 km thick chamber that supports a 400 m mid-segment high ($\Delta\rho$=200 kg/m^3) must thin about 2 km to a thickness of 1.85 km at a ridge tip that is 200 m deeper.

A magma chamber containing only melt will not exist continuously.

With changes in the flux of new material from below, the thermal conditions change and crystallization will occur to varying degrees. The isostatic calculations depend only on the total amount of low density material beneath the ridge. Therefore, the relation between ridge height and chamber thickness in Figure 4.6 can be expanded to include various degrees of crystallization in a larger chamber. In order to calculate the effective density of a magma chamber that has partially crystallized, the density of the solid component must be known. Realistically the density of the crystals will vary with melt composition, temperature and pressure. But it is reasonable to assume an average density for the calculations and, thereby, to show the general effect of magma solidification on isostatic balance of the ridge.

Grove and Bryan (1983) report the modal proportions of olivine, pyroxene and plagioclase for various degrees of crystallization of MORB melts. Assuming a density of 2700 kg/m^3 for the liquid phase, 3400 for olivine, 3200 for pyroxene and 2700 for plagioclase, an effective density of the melt + solid is calculated. Figure 4.7 shows these effective densities as a function of degree of crystallization of the magma for the data of Grove and Bryan (1983). Using the least-squares line fit of all the points, a single density can be considered to represent a specific degree of crystallization. With this information it is possible to determine the size of a magma chamber, of a specified degree of solidification, that is equivalent to a smaller chamber containing 100% melt. Figure 4.8a shows that for melt-only chambers of 1, 2 and 3 km thickness, larger chambers of up to 80, 60 and 40 percent crystallization, respectively, will support corresponding ridge

elevations. Examples of the increase in chamber size with increased solidification are shown in Figure 4.8b.

Summary of results. It has been shown that both the subaxial asthenosphere model and the crustal magma chamber model are viable in terms of their ability to support an axial ridge of the height observed along the EPR. Reasonable input values of density and depth parameters, as determined from petrologic and geophysical data, result in isostatically balanced ridge topography. Subcrustal melt contents of 10-25% can support a ridge axis of 300-400 m height and a decrease of 5-10% in subaxial melt content can account for the deeper ridge tip. A magma chamber 2.5-4.0 km thick can maintain 300-400 m ridge elevation and a 1-2 km thinning of the chamber towards the ridge tip results in a decrease in ridge height of about 200 m.

At this point it is important to check that these density structure models, determined only on the basis of mass balance, are consistent with gravity data. In order to match the small positive free-air gravity anomaly observed over fast spreading ridges, Madsen et al. (1984) show that a negative mass anomaly of the order 1 X 10^6 kg must be present below the narrow axial ridge. Therefore the density structures determined in this study to be capable of maintaining the ridge axis elevation can be checked for consistency with the gravity data. In as much as the Madsen et al. model (1984) continues to be viable as new data are considered, the density structures computed here that give appropriate mass anomalies can be judged as acceptable choices for model ridge structures. All density structures determined to isostatically maintain ridge heights of 200 m or greater have mass

anomalies of the order required by the model of Madsen et al. (1984). Therefore I conclude that these ridge models are suitable as framework for inferring actual density structure.

So far only single columns at the mid-segment high, off-axis or at the tip have been considered. Clearly, to fit the actual ridge profiles one could (nonuniquely) vary each of the depth and/or density parameters between the three columns to achieve an isostatically balanced density structure that is continuous.

In this section a framework has been established in which the scale of topographic dependence on the underlying density structure can be understood. The next step is to apply this to actual ridge topography and to explore the magmatic processes implied by each model for a given structure.

a. SUBAXIAL ASTHENOSPHERE MODEL: constant thickness crust

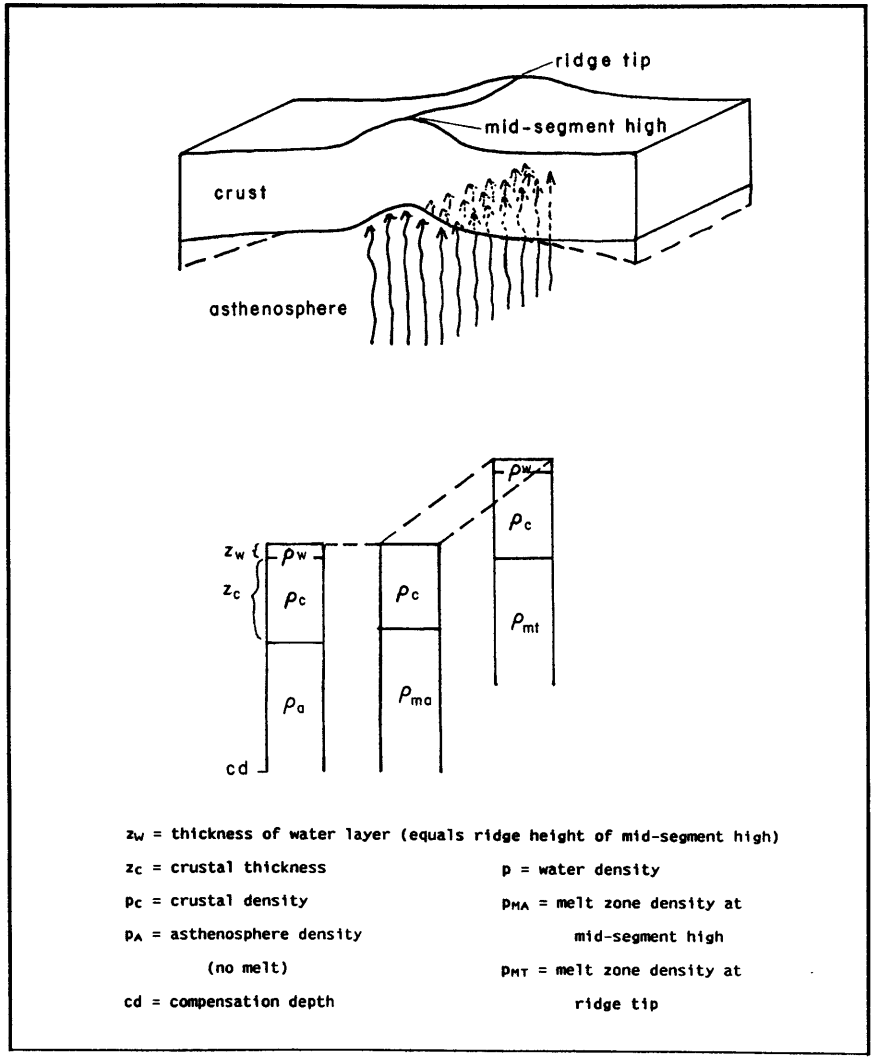

z_w = thickness of water layer (equals ridge height of mid-segment high)

z_c = crustal thickness

ρ_c = crustal density

ρ_A = asthenosphere density (no melt)

cd = compensation depth

ρ = water density

ρ_{MA} = melt zone density at mid-segment high

ρ_{MT} = melt zone density at ridge tip

b.

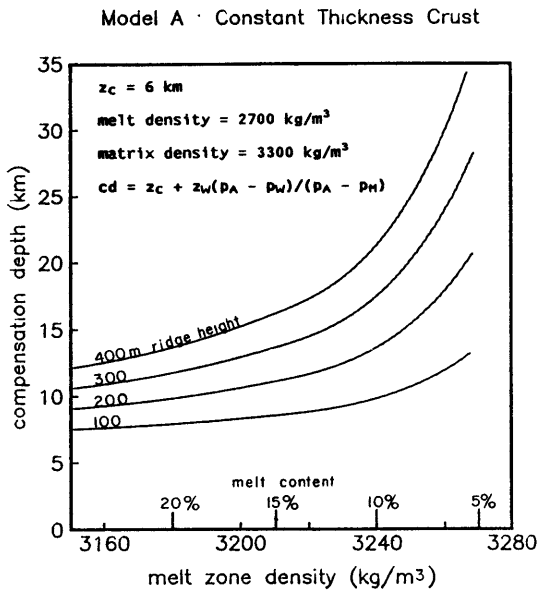

4.1 Model A with constant thickness crust. a) Block cartoon of model and corresponding mass columns for mid-segment high, ridge tip and off-axis regions. Density and depth parameters are labeled on the columns and defined below. b) Relation between melt content of subaxial region and required depth of compensation for isostatically supported ridges of various heights. Assumed values of depth and density are shown at upper left.

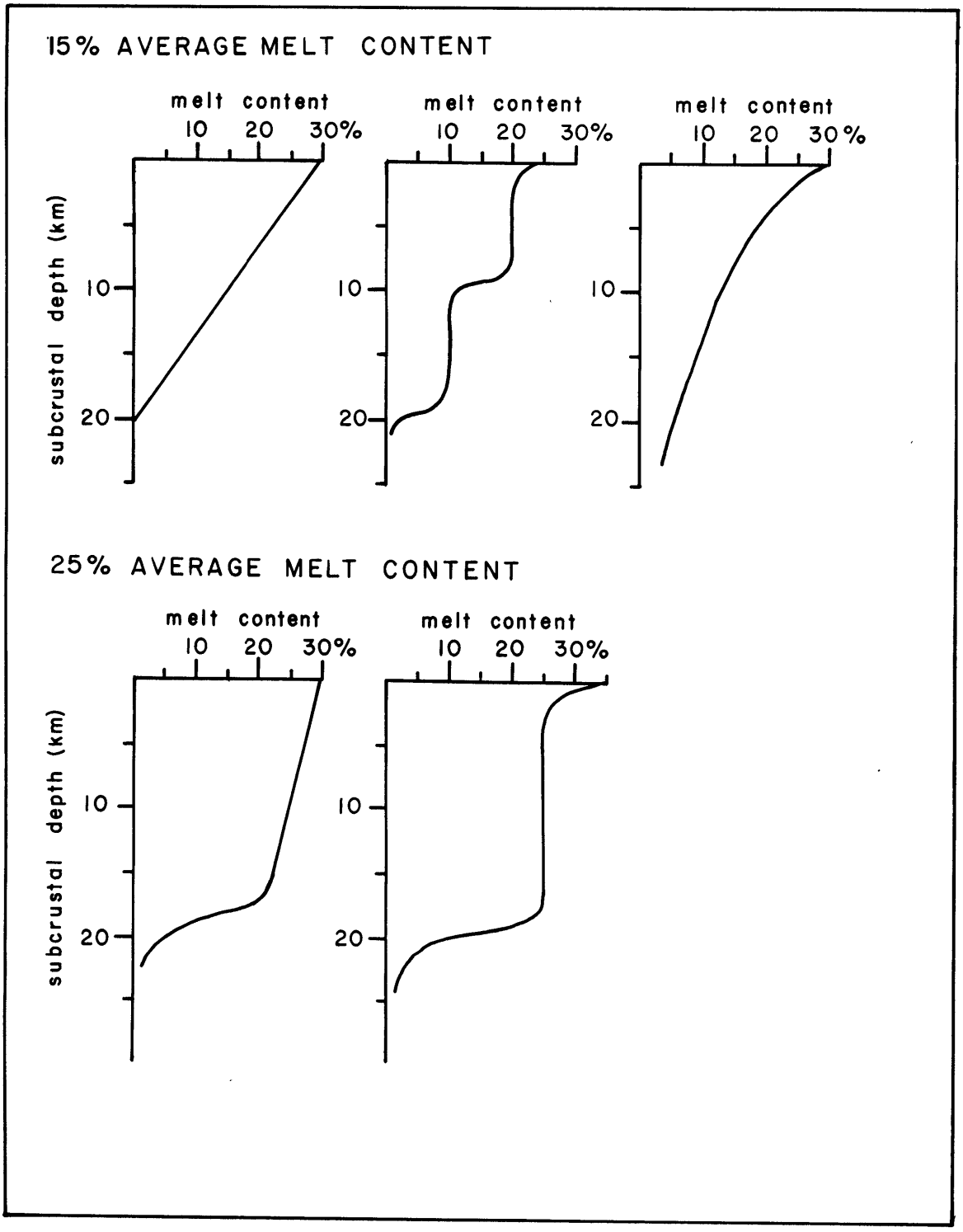

4.2 Examples of subaxial asthenosphere melt distributions which can be represented by an average melt content of 15% (upper) and 25% (lower) over the subcrustal depth range shown.

a. RIDGE STRUCTURE: thin axial crust

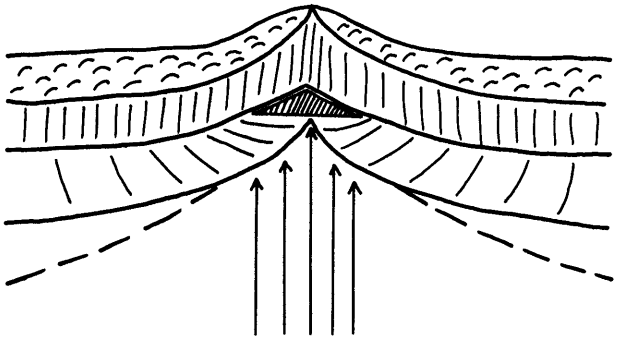

b. MASS COLUMNS: variable thickness crust (cross-strike)

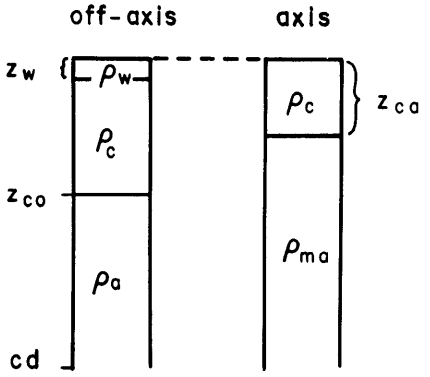

z_W = thickness of water layer (equals ridge height)

z_{cA} = thickness of axial crust

z_{co} = depth at base of off-axis crust

densities are the same as in Figure 4.1

4.3 Model A with crust thinner at the ridge axis than off-axis. Cartoon of subaxial geologic structure, based on Cann (1974), which accounts for thinner axial crust. Corresponding mass columns for the axis and off-axis locations are shown below with depth and density parameters labeled and defined.

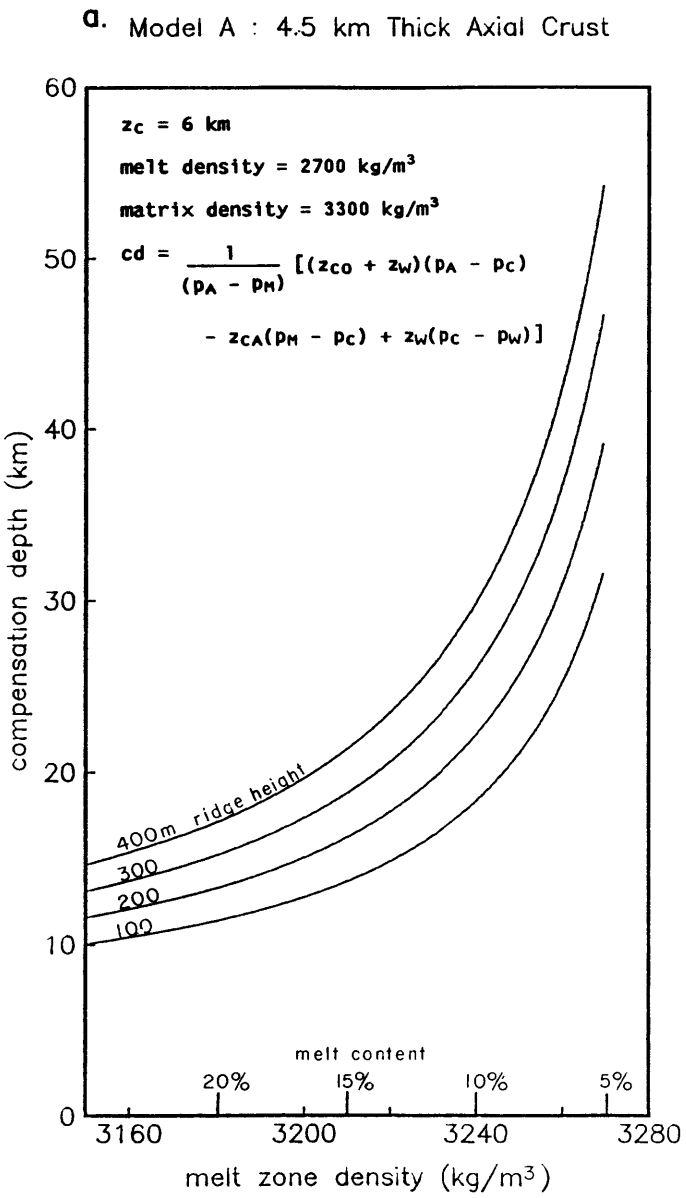

4.4 Effect of varying thickness of axial crust - Model A. a) Relation between melt content of subaxial asthenosphere and required depth of compensation for isostatically supported ridges of various heights assuming a 4.5 km thick axial crust and a 6 km thick off-axis crust. b) Relation between assumed thickness of axial crust and required depth of compensation for various ridge heights and two examples of subaxial melt content. Solid lines indicate 25% melt in subcrustal region, dashed lines indicate 15% melt. Axial thickness of 6 km is constant thickness case (Figure 4.1).

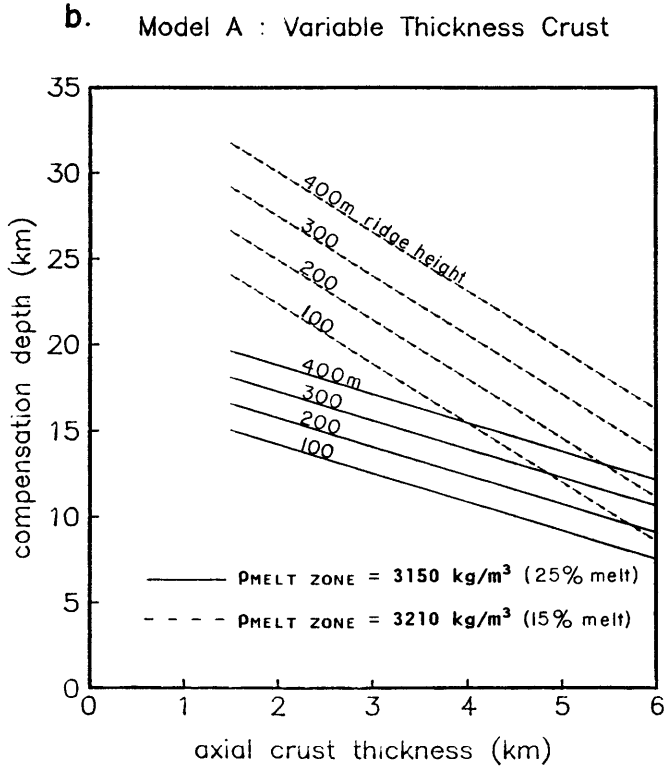

a. AVERAGE DENSITY OF VARIOUS CRUSTAL CONFIGURATIONS

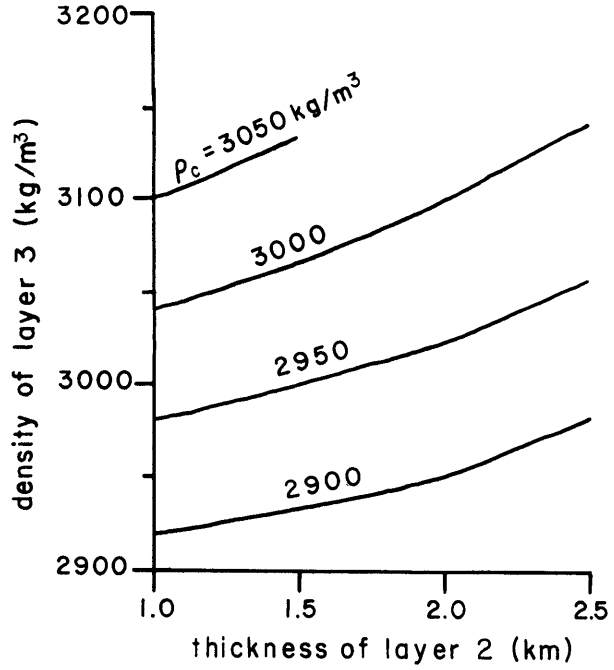

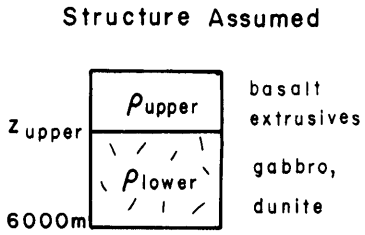

basalt = 2800 kg/m³
gabbro = 2950
dunite = 3400

b.

$$\rho_{lo} = [(6.0)\rho_c - z_{up}(2800)]/(6.0 - z_{up})$$

$$z_{up} = 6.0(\rho_{lo} - \rho_c)/(\rho_{lo} - 2800)$$

c.

EXAMPLES OF CRUSTAL STRUCTURE FOR AVERAGE DENSITY 2950 kg/m³

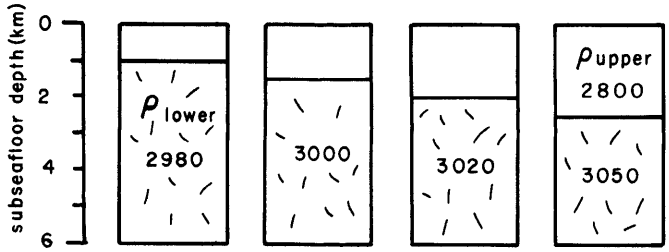

4.5 Average crustal densities for a range of crustal structures. a) Relation between thickness of basalt layer and effective density of gabbroic layer for various assumed average crustal densities (ρ_c). Cartoon at right shows depths and density parameters. Densities assumed for representative rock types are listed below. b) Equations relating: thickness of layer 2 to various assumed densities; effective density of layer 3 to thickness of layer 2 and average crustal density. c) Diagram of several examples of crustal structure for which the average crustal density is 2950 kg/m³.

a.

CRUSTAL MAGMA CHAMBER MODEL

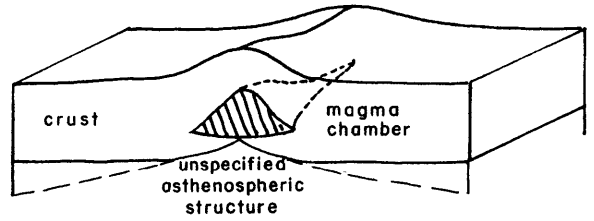

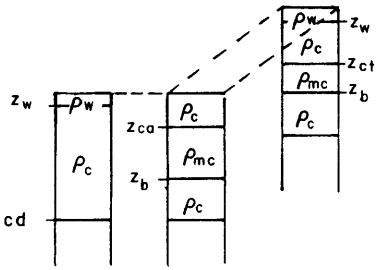

z_{CA} = depth of top of magma chamber at mid-segment high

z_{CT} = depth at top of magma chamber at ridge tip

z_B = depth at bottom of magma chamber

ρ_{MC} = density of magma chamber

other variable are the same as in Figure 4.1

b.

Dependence of Ridge Height on Chamber Thickness

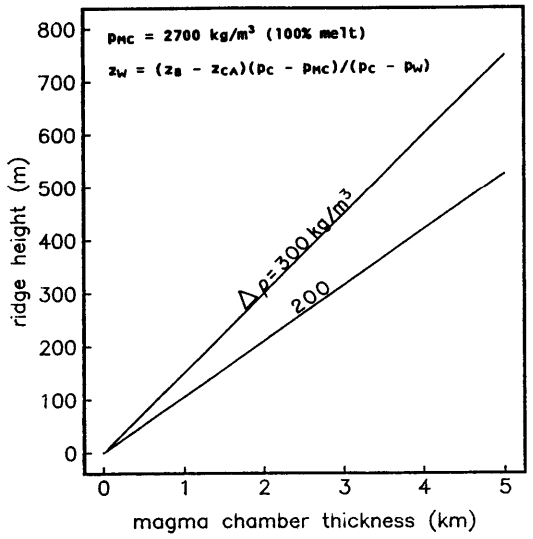

4.6 Model B. a) Block cartoon of model and corresponding mass columns for mid-segment high, ridge tip and off-axis regions. Depth and density parameters are labeled and defined below. b) Relation between thickness of axial magma chamber, containing only basaltic liquid, and height of the ridge which it can isostatically support. Curves for density contrast (between melt in chamber and surrounding crust) of 200 and 300 kg/m³ are shown. Assumed values of depth and density are listed at upper left.

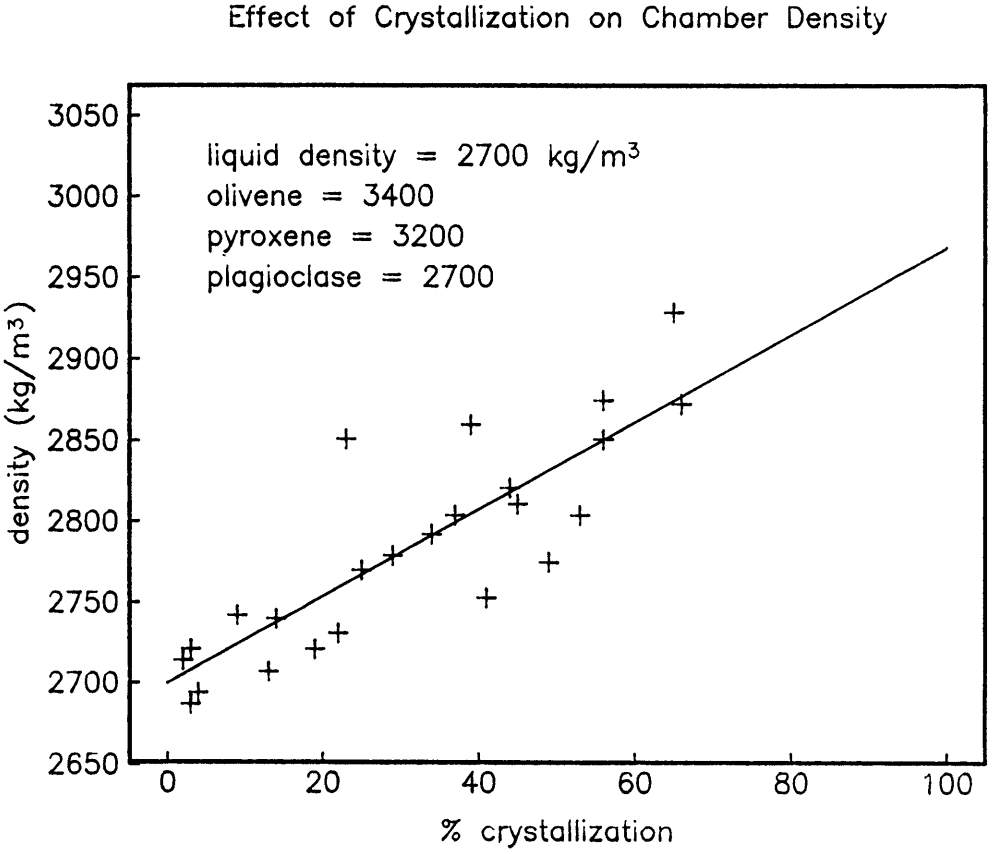

4.7 Relation between amount of crystallization in magma chamber and effective density of that chamber. Calculations are based on phase proportions from Grove and Bryan (1983) and the densities listed in upper left. Least-squares fit of all data points is shown.

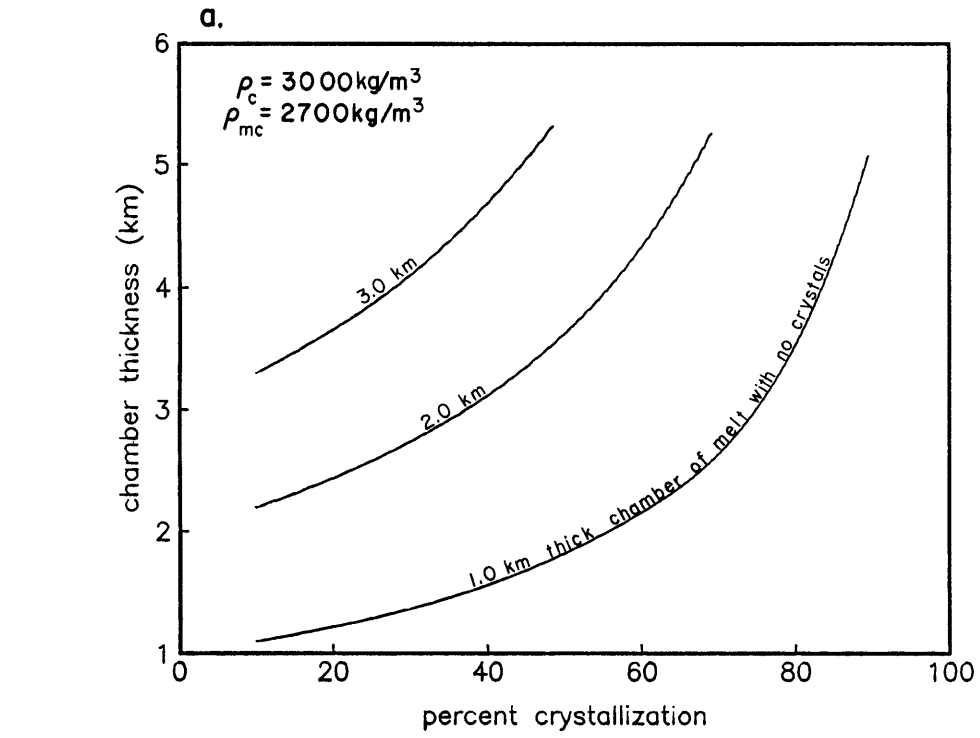

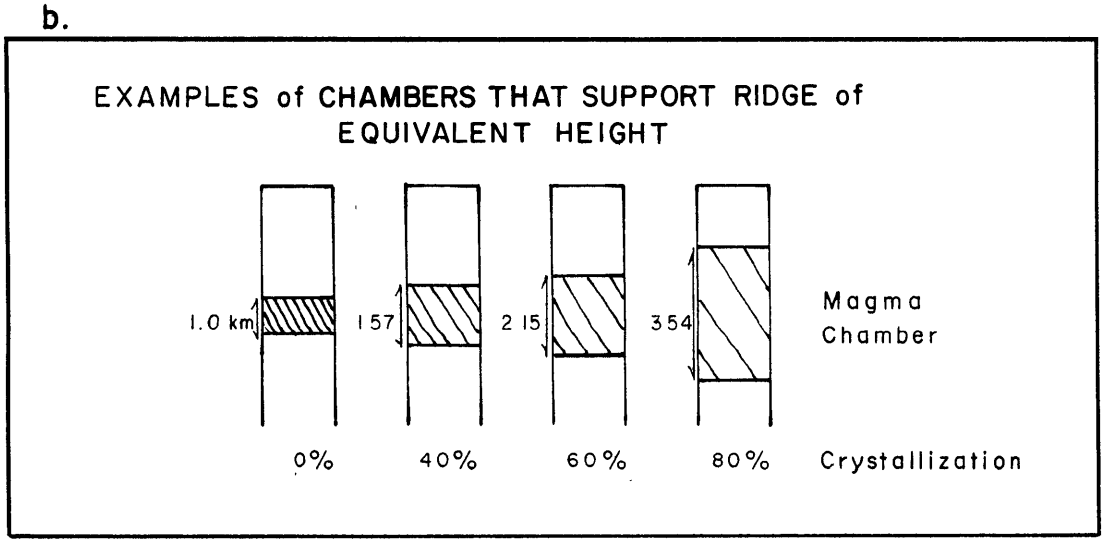

4.8 Equivalent mass balance magma chambers of various degrees of crystallization. a)Relation between degree of crystallization in chamber and thickness of that solidifying chamber which will support a ridge equivalent to that supported by chambers of various thicknesses containing only melt. b) Examples of chambers, crystallized to 40%, 60% and 80%, that can support a ridge of the same height as that supported by a 1 km thick, pure melt chamber.

5. Discussion of Results

If the assumption that axial ridges at fast spreading MORs are isostatically supported is valid then ridge elevation and ridge volume are direct indicators of the amount of melt present in the subaxial region. Elevation is a function of the melt content beneath a given point on the ridge and volume reflects the total amount of melt below the ridge. The melt may be distributed subcrustally, in the interstices of the subaxial asthenosphere, or it may accumulate in a crustal magma chamber. Each of these possibilities carries its own implications for the structure and magmatic processes at MORs, and there may be complications associated with requiring either one to be the sole supporter of ridge morphology.

In section 1 several previous models of subaxial ridge structure were discussed, the reason was twofold: 1) to review the various models of subaxial asthenospheric melt and crustal magma chambers together so that they could easily be compared and contrasted; 2) to point out the consistently one-sided (one-regioned) approach taken by previous modelers. The results of section 4 show that melt in either region (crust or subaxial asthenosphere) can support an axial ridge of the size observed along the EPR. No presently available data shows conclusively that one or the other model can be ruled out. Subaxial asthenospheric melt could be equally as important as crustal magma chambers in supporting a given section of axial ridge. Yet, a closer look at the melt distributions predicted by the mass balance calculations provides further insight into the magmatic systems implied by each model, allowing some qualitative constraints to be put on their acceptability.

Subcrustal melt distributions. What is implied by the model of an axial ridge supported by subcrustal melt, distributed over a depth range of 10 to 20 km, is that the melt zone is extremely narrow. The width of the melt zone must approximately coincide with the width of the ridge which, at the EPR, is typically 3-7 km. In the previous section it was shown that, on average, 10% to 25% melt within the asthenospheric interstices is necessary to maintain a 300 to 400 m high ridge if the depth of compensation is less than 15 km. A bathymetric cross section of the two ridges at the 5°30'N OSC, a representative cross-sectional profile through a large offset OSC, is shown in Figure 5.1 with the corresponding subaxial melt contents drawn below, based on the results of the last section. Although the isostatic density structures are suitable to the ridge system in general, by studying the subcrustal structure indicated at OSCs it becomes clear just how distinct the zone of rising melt must be. Regions of melt 3 to 5 km wide appear to persist separately, as indicated by the presence of the deep overlap basin between the respective ridges, within about 6 km of each other. Such a notion would be unacceptable under general models of asthenospheric upwelling beneath the ridge. But, with a model of melt migration by some mechanism of flow through cracks or through a porous medium, it is quite possible that the subaxial melt zone is rather narrow. The question this brings up is whether a significant amount of melt is only generated within this narrow zone or whether it is generated in a broader region at depth and then channeled into the narrow subaxial zone. Models of Rayleigh-Taylor type gravitational instability suggest that it is possible to channel melt that exists

initially in a broad region (Whitehead et al., 1984; Crane, 1985; Schouten et al., 1985).

The fact that ridges of different width can exist so close together, such as in the example shown in Figure 5.1 suggests the existence of some influence on the system by non-asthenospheric processes, perhaps plate spreading rate. Approximately the same amount of melt is present below each ridge at this latitude (Figure 5.1) but the western ridge has a maximum melt content of 10% across about 2 km below the axial peak whereas the eastern ridge has a maximum of 20% across less than 1 km. It seems unlikely that the temperature and/or mantle composition at depth are sufficiently different to result in local variation in the degree of melting which might produce these different melt concentrations. The similar volumes but different distributions of melt beneath the two ridges suggest that the melt is produced under similar conditions at depth but is channeled differently as it rises. The mechanism by which this might occur is unclear. Conceivably the stress regime below ridge tips that are spreading at different rates might be different enough to affect the melt migration patterns.

According to the subaxial asthenosphere model, a decrease in melt content of 5-10% occurs along-axis from the mid-segment high to the ridge tip. This could indicate two things. One is that the temperature regime at depth below the ridge tip is cooler than that beneath the mid-segment high, therefore less melt is generated and/or less rises steadily through the asthenosphere (Figure 5.2a). Since the distance between the mid-segment high and the ridge tip is of the order of 30-50 km this variation in mantle properties seems more plausible than for the

case above where variation over 5 km distance was questioned. Based on the occurrence of basalts enriched in Fe, Ti and light rare earth elements, Langmuir and Bender (1977) suggested that less melting occurs at depth near ridge-transform intersections. Although they tend to take the approach that it is the juxtaposition of the ridge and the cold plate edge at the transform that causes the cooler temperature regime, it may be more appropriate to view the difference in mantle melting as the cause for the persistence of the ridge discontinuity. With this view it seems plausible that a region of lower melting could be associated with OSCs as well as fracture zones.

The other possibility indicated by the lower melt content beneath the ridge tip is that melt rises centrally from depth and then flows longitudinally at shallower levels decreasing in volume away from the feeder conduit (Figure 5.2b). Models of propagating rifts (Phipps-Morgan and Parmentier, 1985) and of the migration of axial magmatism (Schouten et al., submitted) suggest that this might occur to some degree. Phipps-Morgan and Parmentier (1985) develop a model of longitudinal asthenosphèric flow in a subaxial conduit to explain the steepness of the ridge tip and the rate of rift propagation at Galapagos 95.5°W. The OSC system can be shown to be geometrically self-similar to the Galapagos propagating rift and the EPR ridge tips do have axial slopes that are greater than those of the rest of the segment (Lonsdale, 1983; Macdonald et al., 1984). Use of this model suggests an overall propagation of the OSC which is a controversial subject at present (Lonsdale, 1985; Schouten et al., submitted; Schouten et al., 1986; Macdonald et al., 1984; Sempere and Macdonald, 1986; Macdonald et al.,

1986). But, Phipps-Morgan et al. (1985) show that, if propagation occurs, the axial bathymetry of the 5°30'S OSC can be explained with their model. They show that the western ridge should be propagating to the north and the eastern ridge should be presently stable.

Further evidence of along-axis asthenospheric motion relative to the plate boundary may be found in the off-axis morphology. Schouten et al. (submitted) show that several bathymetric features, many of them not well surveyed, trend in a direction that is predicted by global plate motion models to correspond with the movement of the plate boundary over stationary regions of mantle upwelling.

In short, there are several indications that along-axis motion of asthenosphere or, perhaps, the melt contained within it may occur. No one model has received general acceptance at this time and the results of this study cannot be used to evaluate the processes implied by each. What is clear from the isostatic calculations is that significant along-axis variations in the properties of the subaxial asthenosphere are necessary to support the observed axial ridge (model A assumed). Some form of longitudinal mantle and/or melt flow could provide a mechanism for maintaining these variations.

Melt accumulation in a crustal magma chamber. In contrast to modeling subaxial asthenospheric motion, modeling the ridge axis as a result of melt in a crustal magma chamber is somewhat better constrained. The melt occurs within the crust and, in a time averaged sense, the motion of the melt is assumed not to be important. The size of a magma chamber necessary to support a 300 to 400 m high ridge ranges from 2.5 to 4.0 km thick and 3 to 5 km wide, depending on the density contrast between the

melt and the surrounding crust and the width of the ridge, respectively. Figure 5.1 gives an example of the chamber that could support the ridge topography at the 5°30'N OSC. The sizes indicated assume 100% melt in the chamber and they must be increased significantly if there is crystallization within the chamber as discussed in the previous section. It is not presently possible to convincingly delimit the size of an axial magma chamber but there are indications from gravity models (Madsen et al., 1984) and petrologic data (Langmuir et al., submitted) that continuous, large chambers are not the norm along the EPR. Madsen et al.'s (1984) gravity inversion results favor a small low density body within the crust, therefore, the 3-4 km thicknesses required to isostatically support the ridge with a magma chamber may be too large. Langmuir et al. (submitted) suggest that axial magma chambers are discontinous along the rise based on the variable petrology and geochemistry of dredged basalts. They show that even small offsets or bends in the ridge axis are associated with compositional changes indicative of the existence of separate magma chambers to either side of the morphologic discontinuity. This would not necessarily preclude the existence of a thick but short chamber within a ridge section, but the compositional variability, in general, suggests that a chamber large enough to be well buffered is not maintained. Unfortunately, the presently available seismic data are unable to resolve the thickness of the low velocity region for which an upper reflector is seen. Perhaps the application of seismic tomography techniques to the problem will help resolve whether 4 km thick magma chambers with low degrees of crystallization do in fact exist.

Nevertheless, the petrologic and multichannel seismic data discussed in section 1 show rather conclusively that axial magma chambers do exist. What is suggested by the mass balance calculations is that a chamber of reasonable size (perhaps 1/2 to 2 km thick) would certainly contribute to the axial ridge elevation but that it is unlikely that the shallower ridges are supported solely by a crustal magma chamber.

Additional indications that a crustal magma chamber is unlikely to be the sole supporter of ridge topography are found when ridge volume is considered. In Figure 3.3 the axial volume of several sections of the EPR is shown to range from about 2×10^6 to about 4×10^6 m^3/m. The amount of melt necessary to isostatically balance this volume, whether it be contained in a magma chamber or distributed subcrustally, can be estimated. The density contrast between the axial ridge and the seawater is about 1800 kg/m^3, between the melt and its asthenospheric matrix $\Delta\rho \simeq 600$ kg/m^3 and between the magma chamber and the surrounding crust $\Delta\rho \simeq 250$ kg/m^3. Therefore, for a ridge volume of 3×10^6 m^3/m, the subcrustal melt volume required is 9.0×10^6 m^3/m. This could reasonably be distributed as 18% melt in a 5 km wide zone of about 10 km depth or as 10% melt in a region 5 km wide and 18 km deep. The amount of melt in a magma chamber that would balance the same ridge volume is more than twice as much (2.2×10^7 m^3/m) and implies a chamber of pure melt 5.3 km average thickness (thicker at the axis and thinner on the flanks to match the ridge elevation) and 5 km wide. For a ridge volume of 2×10^6 m^3/m, a chamber about 3.0 km thick and 5 km wide is needed. The latter seems more plausible than the former in that, as discussed above, a 4.3 km thick chamber of pure melt would

probably not produce the petrologic and gravity signatures observed.

Thus far, much of the discussion has been applicable to fast spreading MORs in general. A few comments on the mass balance results that are specific to OSCs are also warranted.

Implications for large offset OSCs. The subaxial density structure of isostatically supported ridges that overlap, and the magmatic processes implied by their proximity at OSCs, can be understood in terms of the results of section 4. In Figure 5.3 several cross-sectional bathymetric profiles from the 5°30'N OSC are shown, each with the corresponding density structure determined for model A and model B. At 5°24' the melt region is broad with a central melt maximum and a smaller high to the east. At 5°31' two separate melt regions exist but at 5°37' the mass balance results show that there could be a continuous, though centrally attenuated, region of melt below the ridges. At 5°41' a single melt region, containing about 2/3 the amount of melt contained below 5°24', is indicated. The cross-section at 5°37' is interesting in that it indicates the possible communication of melts below the two ridges. Petrologic sampling of OSCs is not yet extensive enough to determine whether basalts from the very tip of a (western, in this case) ridge are similar to those found on the adjacent (eastern) ridge. Certainly the differences between the western ridge basalts and the eastern ridge basalts at 11°45'N (Thompson et al., 1985) indicate that the magma batches are quite distinct there, where the two ridges are still morphologically distinct. But, any future petrologic data from regions where one ridge terminates very close to the axis of the other ridge (11°40'N, 8°56'N and 5°25'N, for example), will provide important

constraints on the structure of the melt region.

An important observation, in light of the ridge volume estimates as well as the mass balance results, is that the shallower ridge segments at the OSCs appear to be volcanically inactive at present. Deep tow data at the 9°03'N OSC (Sempere and Macdonald, in press), ANGUS (Thompson et al., 1985) and ARGO (Hekinian et al., in prep) data at the 11°45'N OSC reveal sedimented pillow basalts with no sign of significant recent extrusion or hydrothermal activity at the western ridge tips. This is interesting since the volume of these ridges exceeds that of the eastern, deeper and broader ridges at both OSCs (Figure 3.4a). The higher volume suggests that a greater amount of melt is present below the shallow, yet apparently inactive, western ridges. This could indicate that melt is currently being stored subcrustally or in a magma chamber but that extension is not occurring at these ridges so little or no magma is being extruded. Another possibility is that the ridge elevation is great enough so that the underlying magmatic system can no longer maintain the hydraulic head needed to get the magma up to the crestal seafloor. In this case lateral dike injection should occur so that the magma could extrude at a lower elevation down axis. At the western ridge tips no recent activity has yet been found, so lateral injection of the magma must occur to the south if at all. There is some evidence that the lavas from the mid-segment high on the western ridge of the 11°45'N OSC are being extruded to the south at 11°15'. Thompson et al. (1985) show that basalts recovered from 11°15' have geochemical and mineralogical signatures similar to basalts from the mid-segment high at 11°30'. The reason for such implied directionality of magmatic

activity is unclear, though it could be related to along-axis migration of the magmatic system as a whole.

If melt is accumulating in a magma chamber beneath the shallower western ridges there must be sufficient influx of new material so that the temperature maintains the amount of melt necessary to support the ridge elevation. If the chamber were 'stagnating' (Lonsdale, 1985; Macdonald et al., 1984) and therefore, presumably, cooling, the overall density of the chamber should increase (see discussion in previous section and Figure 4.7) and there would be a corresponding deepening of the ridge.

The magnitude of the elevation difference between the two ridges at large offset OSCs is typically about 100 m. This could be accounted for by melt accumulation in a 1 km thick magma chamber. In contrast, it is difficult to envision an increase in the amount of subcrustal melt as being responsible for the shallower, yet apparently inactive, western ridges. As mentioned earlier in this section, it seems unlikely that temperature and/or compositional conditions at depth are sufficiently different below the two ridges to produce different amounts of melt. If the same amount of melt is produced at depth but it is retained in the asthenosphere below the shallower ridge tip (perhaps due to a period of nonextension at the surface) there would have to be some reason for the melt to remain there as opposed to flowing along-axis to extend the ridge.

Comments on previous OSC models. The ridge volume and mass balance results of sections 3 and 4 bear directly on previous models of OSC structure and evolution. Lonsdale (1983, 1985) proposed that the whole

OSC is underlain by a single, 'dog-legged' magma chamber with the overlap basin resulting from collapse of the lid over the center of the chamber. The subaxial melt distributions predicted in section 4 and illustrated in Figures 5.1 and 5.3 show that this is unlikely to be the case. Rather than a single, continuous magma chamber, the mass balance results for model B suggest that, at least for part of the overlap region, the eastern and western ridges are supported individually. Admittedly, this is a function of the choice of reference depth, the uncertainties of which were discussed in section 3. But, at 5°30'N the reference depth would have to be taken at 3450 m to accommodate a chamber 1/2 km thick beneath the overlap basin which would connect the subaxial chamber across the OSC. This, in turn, would require a magma chamber, of pure melt, over 6 km thick to support the axial ridges to either side - an unlikely configuration.

Macdonald et al. (1984) suggested that OSCs result when two magmatic pulses, centered beneath the mid-segment highs of the eastern and western ridges respectively, do not meet at their distal ends due to either crustal heterogeneity or differences in the stress field near the tip of each ridge segment. They predict that the western segments of the 9°03'N and 11°45'N OSCs, which appear to be volcanically inactive, are dying off and will eventually be overtaken by the propagating eastern ridge. For this model to work there must be some explanation for the shallow, yet apparently inactive, western ridges which, based on the mass balance calculations, are underlain by a greater concentration of melt and, in some cases, a greater total volume of melt. As mentioned in the previous subsection, it is possible that the melt is

being preferentially extruded to the south of the mid-segment high. Another possibility is that it is extruded outside the neovolcanic zone to form flank volcanoes.

In addition to the problem of apparent inactivity associated with greater melt concentrations at shallower ridges of OSCs, the predictions of the Phipps Morgan and Parmentier (1985) PR model need to be addressed. If their model is indeed applicable to overlapping ridges which propagate, even in the piece-wise manner proposed by Macdonald et al. (1984), the shallower ridges should have a greater driving force to maintain propagation than the broad, deeper ridges. The results of this study can only be used to point out these inconsistencies, it is not yet possible to resolve these questions. Yet, an understanding of the magmatic and tectonic processes at ridge discontinuities is fundamental to the complete understanding of the creation of oceanic crust. Several experiments are possible in which to extend this important research.

Suggestions for further research. Several questions concerning the distribution of subaxial melt, the along-axis flow of asthenosphere, the migration of the OSC system and the variability of the subaxial mantle have been raised here. In most cases, firm conclusions cannot yet be reached without further study though it is suggested that an axial magma chamber is not the only source of low density material that supports fast spreading MORs. Constraints on the dimensions of an axial magma chamber could be attained by a combined seismic tomography and gravity experiment. The seismic velocity structure of the subaxial region could be determined, within the limits ($\pm \simeq 1$ km in the width of the axial low velocity region) of modeling assumptions, by seismically imaging the

ridge along closely spaced (1-3 km) cross-strike tracklines extending 15-20 km out on the ridge flanks. Gravity data, collected concurrently, could be used to check models of density structure and, thereby, to enable better control on the subaxial seismic velocities. In order to provide a regional reference, longer gravity profiles would be needed at a few locations. It would be impractical to attempt such an experiment right at an OSC, due to the structural complexity, but coverage of a ridge section a few km from the overlap and a section at the mid-segment high could reasonably be obtained. Optimally a section in between would also be included, though, logistically, acquiring and processing that much data would be nontrivial.

Recently developed active source eloctromagnetic sounding methods, which are currently being refined to optimize retrieval of seafloor data (Francis, 1982; Lilley, 1986), hold great promise for providing information on subaxial melt distribution in the 2-20 km depth range addressed here. Melt contents as low as a few percent can be recognized and models of interstitial melt geometry can be further tested with such data. This could provide constraints not only on the present melt distributions but also on possible mechanisms of melt migration.

Precisely located petrologic sampling of the neovolcanic zone at intervals on the order of 1/2 to 5 km along a ridge segment as well as on several adjacent segments would provide information on possible communication between magmatic systems beneath ridge tips, or lack thereof. Patterns of magmatic evolution determined from sampling at these intervals - fractionation trends associated with a spatial distribution of basalts for example - would allow the hypothesis of a

continuous, centrally supplied, axial magma chamber to be checked. Models of magma mixing and chamber dynamics could be used to check the limits of chamber dimensions that could produce the observed petrologic variability. Subseafloor drilling of basalts at a series of locations starting at the ridge axis, spaced 10-20 km (1-2 myr at 10 km/myr spreading rate) out as far as logistically reasonable, in the direction of plate spreading would provide an important view of any time evolution of the magma composition. This would bear on models of the migration of subaxial magmatism along MORs and models of ridge propagation at OSCs.

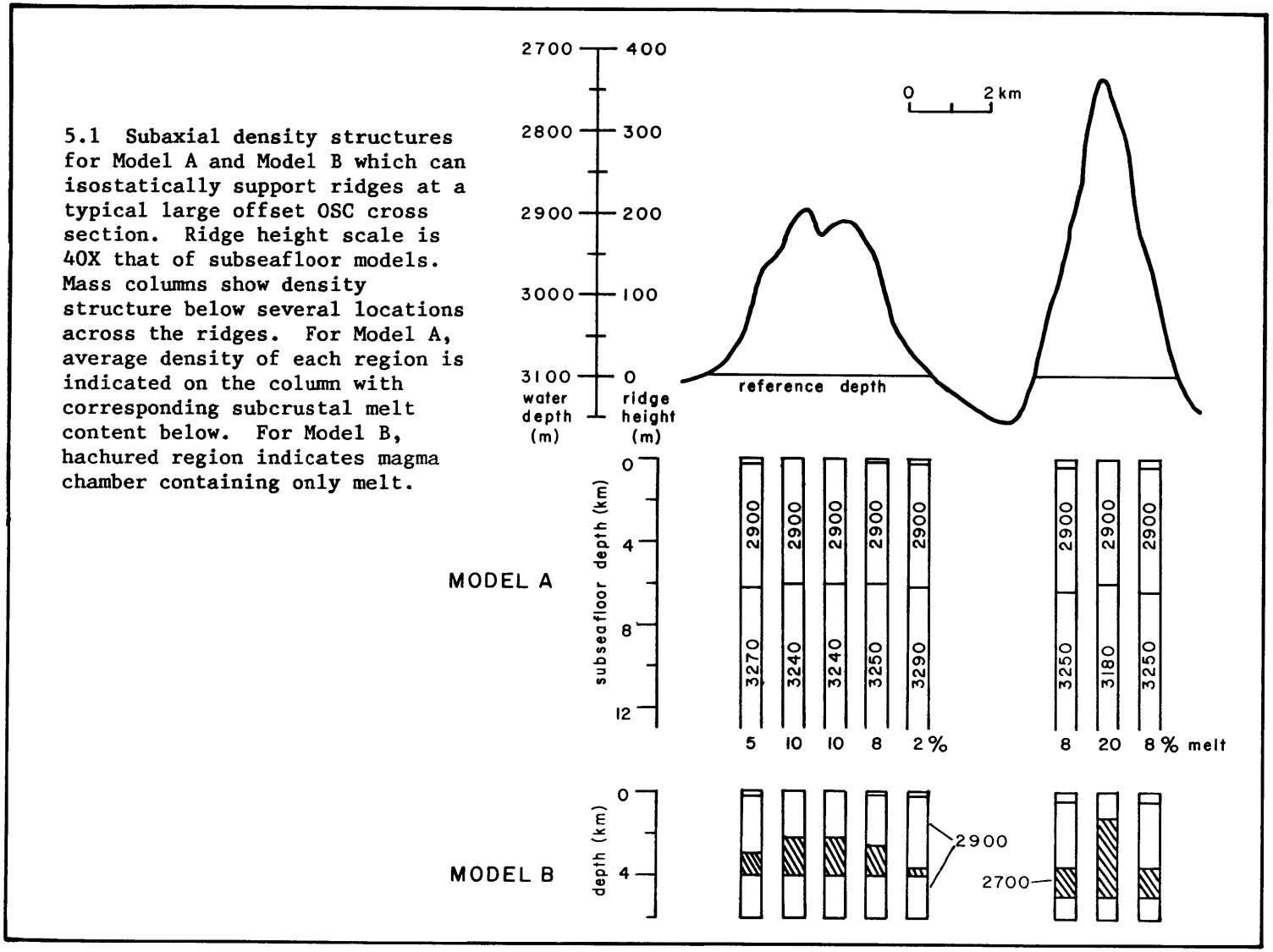

5.1 Subaxial density structures for Model A and Model B which can isostatically support ridges at a typical large offset OSC cross section. Ridge height scale is 40X that of subseafloor models. Mass columns show density structure below several locations across the ridges. For Model A, average density of each region is indicated on the column with corresponding subcrustal melt content below. For Model B, hachured region indicates magma chamber containing only melt.

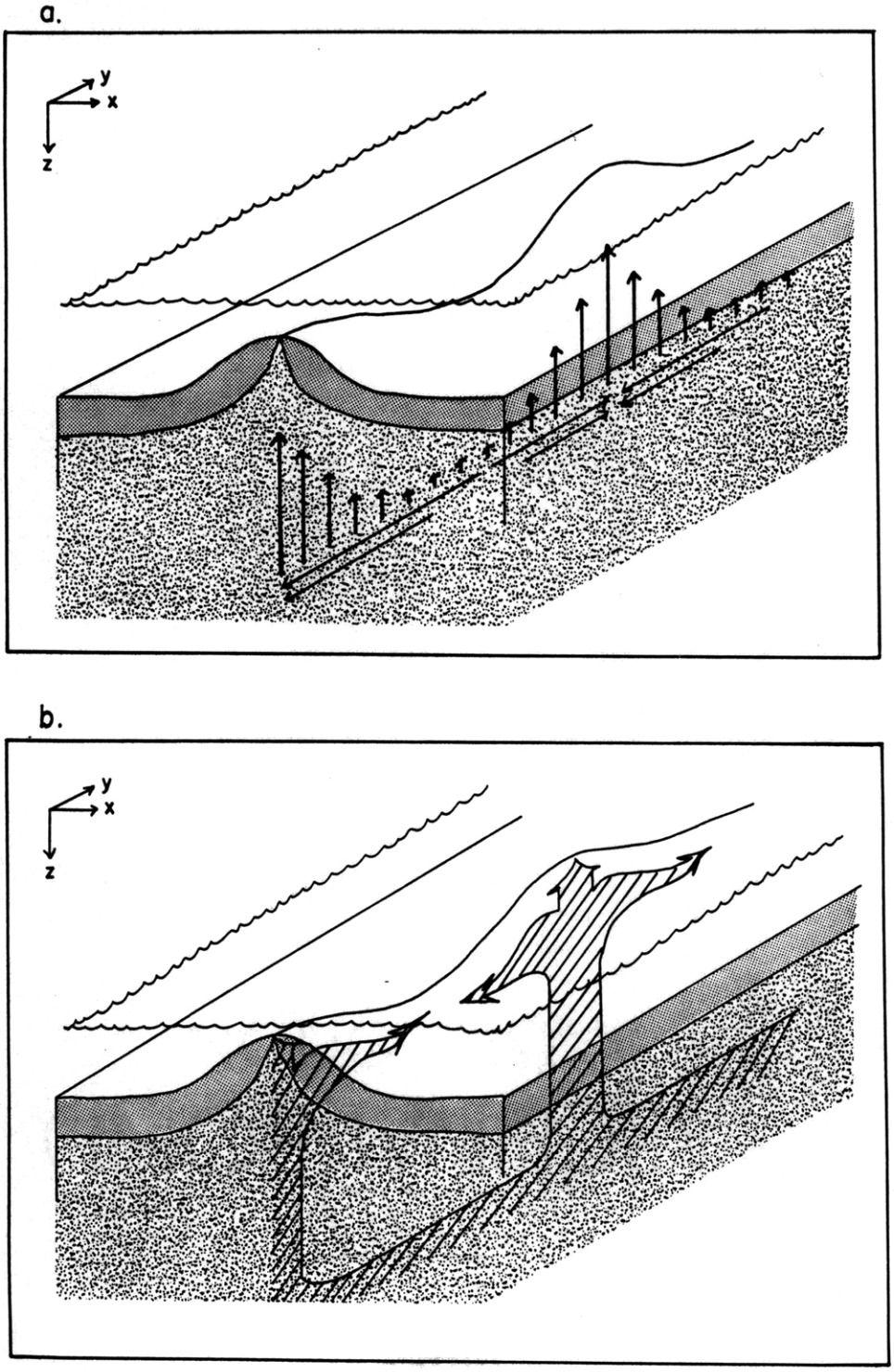

5.2 Schematic drawing of subaxial mid-ocean ridge processes. a) Upwelling concentrated at mid-segment high with upflow reduced along-axis. b) Upwelling in discrete melt zone with subcrustal horizontal flow away from mid-segment high.

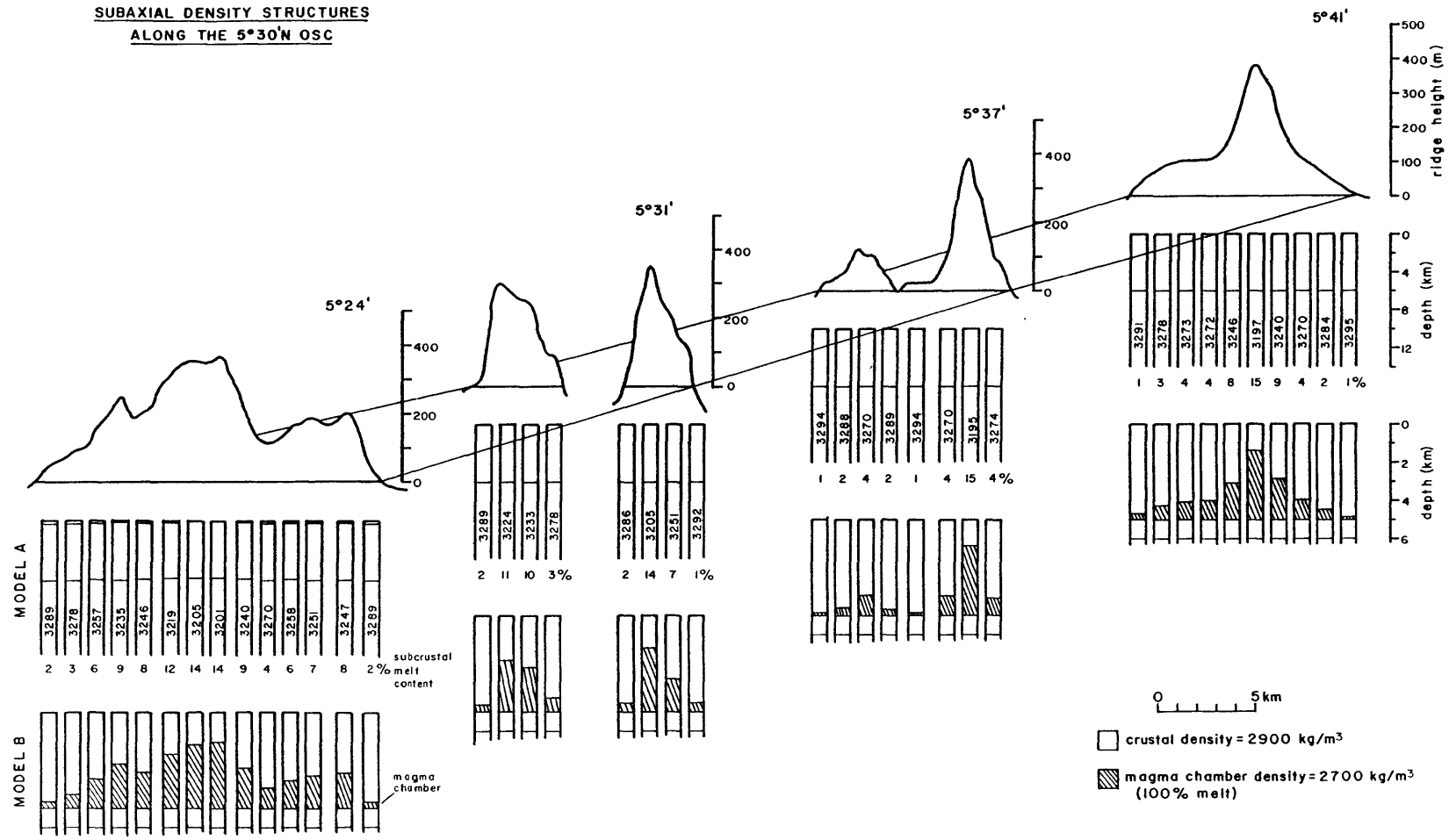

5.3 Series of bathymetric profiles through 5°30'N OSC with corresponding subaxial density structures shown for Models A and B. Format is similar to Figure 5.1 although ridge height scale is 38X that of Model A subseafloor scale, horizontal scale is smaller, and scale for Model B is larger than for Model A.

6. Summary and Conclusions

Previous models of fast spreading mid-ocean ridges fall into two classes: those that explain the surface morphology as a result of subcrustal flow of asthenosphere and the melt contained subaxially; those that attribute ridge structure and volcanism to the accumulation of melt in a crustal magma chamber. This division of emphasis is artificial (typically a function of a given author's approach) and the results of previous studies can be misleading in their neglect of either the crustal or subcrustal region. Nevertheless, the division does provide a useful construct for investigating the possible role of melt located in either region in supporting the 3-7 km wide axial ridge. Two end member models, designed to emphasize, individually, the contribution of the subaxial asthenospheric melt and that of melt in a crustal magma chamber, have been tested for their ability to support an axial ridge. The morphology of ridge segments that terminate at large offset OSCs along the EPR was used to constrain the range of subaxial density structures determined for each model.

Mass balance calculations, based on the assumption of local isostatic compensation of the axial ridge at fast spreading centers, show that both a model of subaxial asthenospheric melt and a model of a crustal magma chamber can be used to explain the magnitude and along-strike variability of the axial ridge.

Estimates of axial ridge volume, made along four large offset OSCs as well as at several other locations along the EPR, range from 1 X 10^6 to 5 X 10^6 m^3/m. The combined volume of the two ridges of the 5°30'N, 9°03'N and 11°45'N OSCs appears to decrease by 30-50% from south

to north. Smaller amplitude volume variability along the eastern and western ridges of the 11°45'N OSC appears to be associated with small offset OSCs and local topography which sometimes correspond to changes in axial basalt geochemistry.

Conclusions are as follows:

1. The subaxial asthenosphere model requires melt contents of 10-25%, distributed throughout the subcrustal region down to 25 km depth, to support the axial ridge. The melt zone is shown to be quite narrow (3-7 km) and a decrease in melt content of 5-10% is needed to fit the deepening of the ridge towards the tips.
2. The crustal magma chamber model supports an axial ridge of 300-400 m height with chamber thicknesses of 2.5-4.0 km, assuming only melt is present. Thinning of the chamber by 1-2 km is necessary to balance the deeper ridge tips. Thicknesses of 3-4 km of pure melt may be on the large side of acceptable chamber thickness and, therefore, the shallower sections of the EPR may not be solely supported by an axial magma chamber.
3. Models of OSC structure and evolution must account for the shallowness of the volcanically inactive western ridge segments at large offset OSCs. Mass balance calculations suggest that these ridges are underlain by a greater melt concentration than the broad, deeper ridge segments, which may contradict models that predict that the shallow ridge is dying off.

References

AHERN, J.J. AND D.L. TURCOTTE,1979 Magma migration beneath an ocean ridge, EPSL, 45, 115-122

CANN, J.R., 1974 A model for oceanic crustal structure developed, GJRAS, 39, 169-187

CRANE, K., 1985 The spacing of rift axis highs: dependence upon diapiric processes in the underlying asthenosphere?, EPSL, 72, 405-414

DETRICK, R., P. BUHL, J. MUTTER, J. ORCUTT, T. BROCHER, J. MADSEN, 1986 MCS imaging of the axial magma chamber along the EPR between 9° and 13° N, EOS, 67, 360

EAST PACIFIC RISE STUDY GROUP, 1981 Crustal processes at the mid-ocean ridges, Science, 213,31-40

EMERMAN, S.H. AND D.L. TURCOTTE, 1984 The mid-ocean ridge axial valley as a steady-state neck, EPSL, 71, 141-146

FORSYTH, D.W. AND B. WILSON, 1984 Three-dimensional temperature structure of a ridge-transform-ridge system, EPSL, 70, 355-362

FRANCHETEAU, J. AND R.D. BALLARD, 1983 The East Pacific Rise near 21-N, 13 N, and 20 S: inferences for along-strike variability of axial processes of the mid-ocean ridge, EPSL, 64, 93-116

FRANCIS, T.J.G., 1982 Ocean floor conductivity measured, Nature, 295, 550

GROVE, T.L. AND W.B. BRYAN, 1983 Fractionation of pyroxene-phyric MORB at low pressure: and experimental study, Contrib. Min. & Petrol, 84, 293-309

HALE, L.D., C.J. MORTON, N.G. SLEEP, 1982 Reinterpretation of seismic reflection data over the East Pacific Rise, JGR, 87, 7707-7719

HEKINIAN, R., J. M. AUZENDE, J. FRANCHETEAU, P. GENTE, W.B.F. RYAN, E.S. KAPPEL, 1985 Offset spreading centers near 12°53'N on the East Pacific Rise: submersible observations and composition of the volcanics, Mar. Geoph. Res., 7, 359-377

HYNDMAN, R.D. AND M.J. DRURY, 1977 Physical properties of basalts, gabbros, and ultrmafic rocks from DSDP leg 37, in P.T. Robinson (ed), Initial Reports of the Deep Sea Drilling Project, 37, 395-401

KLITGORD, K.D. AND J. MAMMERICKX, 1982 Northern East Pacific Rise: magnetic anomaly and bathymetric framework, JGR, 87,6725-6750

KUSHIRO, I., 1980 Viscosity, density and structure of silicate melts at high pressures, and their petrological applications, in R.G. Hargraves (ed), Physics of magmatic processes, Princeton Univ. Press, Princeton, 93-120

LACHENBRUCH A.H., 1973 Differentation and the gravitational driving force for material rising at an ocean ridge, JGR, 78, 825-831

LACHENBRUCH, A.H., 1976 Dynamics of passive spreading centers, JGR, 81, 1883-1902

LANGMUIR, C.H. AND J.F. BENDER, 1984 The geochemistry of oceanic basalts in the vicinity of transform faults: observations and implications, EPSL, 69, 107-127

LEWIS, B.T.R., 1981 Isostasy, magma chambers and plate driving forces on the East Pacific Rise, JGR, 86, 4868-4880

LEWIS, B.T.R., 1982 Constraints on the structure of the East Pacific Rise from gravity, JGR, 87, 8491-8500

LILLEY, F.E.M., 1986 Conductivity of the seafloor, Nature, 320, 19

LONSDALE, P., 1977a Structural geomorphology of a fast spreading rise crest: the East Pacific Rise near 3°25'S, Mar. Geoph. Res, 3, 251-293

LONSDALE, P., 1977b Regional shape and tectonics of the equatorial East Pacific Rise, Mar. Geophys. Res., 3, 295-315

LONSDALE, P. 1983 Overlapping rift zones at the 5.5°S offset of the East Pacific Rise, JGR, 88, 9393-9406

LONSDALE, P., 1985 Nontransform offsets of the Pacific-Cocos plate boundary and their traces on the rise flank, GSA Bull, 96, 313-327

LONSDALE, P. 1983 Overlapping rift zones at the 5.5°S offset of the East Pacific Rise, JGR, 88, 9393-9406

MACDONALD, K.C. AND J.P. FOX 1983 Overlapping spreading centers: a new kind of accretion geometry on the East Pacific Rise, Nature, 302, 55-58

MACDONALD, K.C., J.C. SEMPERE, P.J. FOX, 1986 Long wavelength undulations of MOR axial depth and SEASAT gravity lineations: evidence for convection?, EOS, 67,359

MACDONALD, K.C., H.C. SEMPERE, P.J. FOX, in press Reply: the debate concerning overlapping spreading centers and mid-ocean ridge processes

MACDONALD, K.C., J-C. SEMPERE, AND P.J. FOX, 1984 The East Pacific Rise from the Sigueiros to the Orozco fracture zones: along-strike continuity of the axial neovolcanic zone and the structure and evolution of over lapping spreading centers, JGR, 89, 6049-6069

MADSEN, J.A., D.W. FORSYTH, R.S. DETRICK, 1984 A new isostatic model for the East Pacific Rise crest, JGR, 89, 9997-10,015

MADSEN, J., R. DETRICK, T. BROCHER, P. BUHL, J. MUTTER, J. ORCUTT, 1986 Variations in the morphology and isostacy of the East Pacific Rise between 9° and 14° N, EOS, 67, 360

MCKENZIE, D.P., 1984 The generation and compaction of partially molten rock, Journal of Petrology, 25, 713-765

PALLISTER, J.S. AND C.A. HOPSON, 1981 Samail ophiolite plutonic suite: field relations, phase variations and layering, and a model of spreading ridge magma chambers, JGR, 86, 2593-2644

PARMENTIER, E.M. AND D.W. FORSYTH, 1985 Three-dimensional flow beneath a slow spreading ridge axis: a dynamic contribution to the deepening of the median valley, JGR, 90, 678-684

PHIPPS MORGAN, J. AND E.M. PARMENTIER, 1985 Causes and rate limiting mechanisms of ridge propagation: a fracture mechanis model, JGR, 90, 8603-8612

PHIPPS MORGAN, J., E.M. PARMENTIER, C. TOWER, 1985 Dynamic models of porpagating rifts and overlapping spreading centers, EOS, 66, 356

REA, D.K., 1975 Model for the formation of topographic features of the East Pacific Rise crest, Geology, 3, 77-80

REA, D.K., 1976 Changes in the axial configuration of the East Pacific Rise near 6°S during the past 2 myr, JGR, 81, 1495-1504

SCHOUTEN, H., H.J.B. DICK AND K.D. KLITGORD, submitted Migration of mid-ocean ridge volcanism, Nature

SCHOUTEN, H., H.J.B. DICK, J.A. WHITEHEAD, 1986 Whole-mantle upwelling under spreading centers, EOS, 67, 359

SCHOUTEN, H., K.D. KLITGORD AND J.A. WHITEHEAD, 1985 Segmentation of mid-ocean ridges, Nature, 317, 225-229

SEMPERE, J.C. AND K.C. MACDONALD, in press, Deep Tow studies of the overlapping spreading centers at 9°03' N on the East Pacific Rise, Tectonics

SEMPERE, J.C. AND K.C. MACDONALD, 1986 Overlapping spreading centers: implications from crack growth simulation by the displacement discontinuity method, Tectonics, 5, 151-163

SEMPERE, J.C., K.C. MACDONALD, S.P. MILLER, 1984 Overlapping spreading centers: 3-D inversion of the magnetic field at 9° N on the East Pacific Rise, GJRAS, 79, 799-812

SINTON, J.M., D.S. WILSON, D.M. CHRISTIE, R.N. HEY, J.R. DELANY, 1983 Petrologic consequences of rift propagation on oceanic spreading ridges, EPSL, 62, 193-207

SLEEP, N.H. and B.R. ROSENDAHL, 1979 Topography and tectonics of mid-ocean ridge axes, JGR, 84, 6831-6839

SLEEP, N.H., 1975 Formation of oceanic crust: Some thermal constraints, JGR, 80, 4037-4042

SLEEP, N.H., AND S. BIEHLER, 1970 Topography and tectonics at the intersection of fracture zones with central rifts, JGR, 75, 2748-2752

SLEEP, N.H., 1969 Sensitivity of heat flow and gravity to the mechanism of sea-floor spreading, JGR, 74, 542-549

SLEEP, N.H. and B.R. ROSENDAHL, 1979 Topography and tectonics of mid-ocean ridge axes, JGR, 84, 6831-6839

SPARKS, R.S.J., P. MEYER, H. SIGURDSSON, 1980 Density variation amongst mid-ocean ridge basalts: implications of magma mixing and the scarcity of primitive lavas, EPSL, 46, 419-430

TAPPONIER, P. J. FRANCHETEAU, 1978 Necking of the lithosphere and the mechanics of slowly accreting plate boundaries, JGR, 83, 3955-3970

TELFORD, W.M., L.P. GELDART, R.E. SHERIFF, D.A. KEYS, 1976 Applied Geophysics, Cambridge University Press, Cambridge, p. 62

THOMPSON, G., W.B. BRYAN, R. BALLARD, K. HAMURO, W.G. MELSON, 1985 Axial processes along a segment of the East Pacific Rise, 10°-12° N, Nature, 318, 429-433

WHITEHEAD, J.A. JR., H.J.B. DICK, H. SCHOUTEN, 1984 A mechanism for magmatic accretion under spreading centres, Nature, 312, 146-148